

**Vertical Distributions of PH₃ in Saturn from Observations
of Its 1-0 and 3-2 Rotational Lines**

G.S. Orton¹, E. Serabyn¹ & Y.T. Lee²

2000-8

To Appear in Icarus

¹Jet Propulsion Laboratory, MS 169-237, 4800 Oak Grove Dr., Pasadena, CA 91109

²Caltech, Geology and Planetary Sciences, MS 150-21, Pasadena, CA 91125



Abstract

Far-infrared Fourier-transform spectrometer measurements of the 1-0 and 3-2 PH_3 transitions in Saturn's disk near 267 and 800 GHz (8.9 and 26.7 cm^{-1}), respectively, were analyzed simultaneously to derive a global mean profile for the PH_3 vertical mixing ratio between 100 and 600 mbar total pressure. The far-infrared spectrum is relatively free from spectral interlopers, suffers minimal absorption or scattering by atmospheric particulates, and contains intrinsically weak PH_3 lines that are sensitive to a range of atmospheric depths. The combined spectra are inconsistent with a uniform tropospheric mixing ratio, even with a stratospheric cut-off. They are consistent with a volume mixing ratio of PH_3 that drops from 1.2×10^{-5} at 645 mbar pressure to a value of 4.1×10^{-7} at 150 mbar pressure, a decrease that is linear in \log abundance *vs* \log pressure. The mixing ratio could drop even more quickly at atmospheric pressures below 150 mbar and still be consistent with the data. The mixing ratio may well remain constant with depth for pressures above 630 mbar. The maximum PH_3 mixing ratio in this model is consistent with a $[\text{P}]/[\text{H}]$ ratio in the deep atmosphere that is about a factor of 10 higher than solar composition. Such a model is consistent with rapid mixing up to the radiative-convective boundary and transport by, for example, vertical waves just above this boundary. In the best fitting model, the eddy diffusion coefficient is $\sim 10^4 \text{ cm}^2$ near 630 mbar, and it must increase with altitude. The predominant PH_3 loss mechanisms are direct photolysis by UV radiation and scavenging by H atoms produced by the photolysis.

Introduction

The presence of phosphine in Jupiter and Saturn was not expected in detectable amounts on the basis of equilibrium thermochemical considerations. PH_3 is not chemically stable at temperatures below ~ 500 K (Prinn and Lewis 1975). At the low (< 150 K) temperatures of the sensible atmospheres of these planets, the PH_3 abundance is expected to drop as solid phosphorus precipitates are formed (Fegley and Lodders 1994, Borunov *et al.* 1995). The presence of PH_3 in detectable quantities is most readily explained by assuming that it is mixed upward from the deeper, warmer atmosphere faster than it decomposes chemically. Because of this, PH_3 can act as a tracer for chemical and dynamical properties of the atmosphere.

Phosphine was first suspected as a major influence on Saturn's infrared spectrum by Gillett and Forrest (1974) and was confirmed by high-resolution spectroscopic detection by Bregman *et al.* (1975). Fink and Larson (1977) further confirmed the presence of PH_3 in Saturn through its influence on the $5\text{-}\mu\text{m}$ spectrum. The first quantitative mixing ratio was derived by Tokunaga *et al.* (1980,1981). They derived a value between 0.8 to 1.6×10^{-6} and required that the vertical distribution undergo a sharp cutoff at total pressures below 100 mbar in order to avoid emission cores in the strongly absorbing centers of lines which otherwise sampled the warm "inverted" stratosphere. Using Voyager IRIS spectra from the northern hemisphere, Courtin *et al.* (1984) derived a constant value of $1.45 \pm 0.8 \times 10^{-6}$ for the PH_3 mixing ratio (assuming a mixing ratio of 96% for H_2 after Conrath *et al.* 1984) with a cutoff at pressures lower than 3 mbar. They also noted that the analysis of International Ultraviolet Explorer observations conducted by Winkelstein *et al.* (1983) required a cutoff of the PH_3 mixing ratio at pressures lower than 25 mbar. Many of these results are summarized in Table IV and Fig. 6 of Prinn *et al.* (1984).

Since the time of that review, Noll and Larson (1990) observed and analyzed Saturn's $5\text{-}\mu\text{m}$ spectrum, including a determination of the PH_3 mixing ratio. They fixed its value at 1×10^{-6} , in agreement with previous work, for levels of the atmosphere where the total pressures was less than 400 mbar. This value was consistent with the portion of the spectrum dominated by reflected sunlight. They derived a mixing ratio of 7×10^{-6} for pressures greater than 400 mbar, using a

portion of the spectrum dominated by thermal emission.

All these early results were due to analyses of vibrational-rotational lines. The “pure” rotational far-infrared 1-0 transition at 266.9 GHz was first observed and analyzed by Weisstein and Serabyn (1994). They found a constant tropospheric mixing ratio of $3 \pm 1 \times 10^{-6}$ to be consistent with the depth and shape of the 1-0 line. In order to avoid the appearance of an “emission core” in this line arising from Saturn’s relatively warm stratosphere, they also required a high-altitude cutoff somewhere between 13 and 140 mbar total pressure, above which no PH₃ was present. The utility of this line is that it is sufficiently weak to be sensitive to regions of the atmosphere significantly deeper than the levels to which the middle-infrared vibration-rotation lines are sensitive. Weisstein and Serabyn (1996) also reported the detection of the 3-2 PH₃ transition at 800.5 GHz as part of a line survey, although the analysis of this line was deferred to a subsequent publication. That is, of course, the motivation for the current report.

Even more recently, observations of Saturn were obtained by the Infrared Space Observatory Short Wavelength Spectrometer (SWS) and Long Wavelength Spectrometer (LWS). The most prominent features in the LWS spectra of Saturn between 43 and 197 μm are pure rotational lines of PH₃, all of which have greater strengths than the two lines reported by Weisstein and Serabyn (1994, 1996). The LWS spectra were fit using a constant tropospheric mixing ratio of 7×10^{-6} for pressures greater than 300 mbar, with negligible amounts at lower pressures (Davis *et al.* 1996). Unfortunately, the value of the constant mixing ratio that Davis *et al.* derived is incorrect, as it is based on spectroscopic line parameters taken from the GEISA data base (Husson *et al.* 1994) that has incorrect line intensities for PH₃ rotational lines (Bézard, pers. comm.) The re-analysis of the ISO/LWS data is ongoing. The ISO/SWS data are consistent with a mixing ratio of 2.5×10^{-6} at 300 mbar, assuming (1) a value of 4.5×10^{-6} at the 600-mbar level and deeper in the atmosphere, and (2) a dropoff from the 300-mbar level to a value of 1×10^{-9} at 150 mbar (de Graauw *et al.* 1997). The mixing ratios between these levels are linearly interpolated in logarithmic form vs log of pressure.

Observations

The spectroscopic observations of the 1-0 and the 3-2 lines reported by Weisstein and Serabyn (1994, 1996) form the basis of this paper. Both lines are illustrated in Fig. 1. For this analysis, Fig. 1 the spectra were processed further. For the 1-0 line, the ripple seen in Fig. 4 of Weisstein and Serabyn (1994) was removed by fitting a single-frequency sine wave component to the spectrum. This dramatically cleaned up the spectrum in the vicinity of the 1-0 line (Fig. 1) but made the more distant baseline noisier where the sine wave fit is no longer applicable. The 3-2 line lies near the edge of an atmospheric window and is very broad. Thus, the high-frequency line wing extends across most of the spectral region observed, and most of the distant low-frequency line wing is completely obscured by the terrestrial atmosphere. In addition, the accessible part of the low-frequency wing is likely to be somewhat affected by rapidly dropping atmospheric and instrumental transmission. The baseline is thus difficult to determine. Finally, slight (0.5-GHz) offsets in line frequencies seem to be present. These could arise from imperfect subtraction of the sine wave component in the 1-0 line or an uncorrected baseline curvature below 800 GHz in the 3-2 line, or, less likely, a possible contribution by HCN. However, the absence of even stronger HCN features near the PH₃ 3-2 line rules out this possibility.

The radiance of the 1-0 data were determined by cross-calibration with Venus (Weisstein *et al.* 1994), an object that provided a minimal number of discrete spectral lines. The absolute radiance reported by Weisstein *et al.* (1994) was based on an interpolation of published absolute radiances for Venus. The 270-GHz continuum brightness temperature of 144 Kelvins derived by Weisstein and Serabyn (1984) agrees with earlier broadband measurements (see their Table II) by Courtin *et al.* (1977), Ulich *et al.* (1984) and Werner *et al.* (1978) with an rms difference of ~ 6 Kelvins, consistent with the uncertainties of these measurements. In this spectral region, the very low temperature of Saturn's rings (*cf.* Fig. 3 of Roellig *et al.* 1988), implies that they do not contribute significantly to the total observed radiance. For the 3-2 data near 800 GHz, on the other hand, determining the true continuum radiance, for which a calibration body was not available (Weisstein *et al.* 1996), requires us to fit only the line-to-continuum ratio, scaling the continuum as required by the model.

Model Basis

A radiative transfer code was employed to derive synthetic spectra to match the observations. The code used 20 vertical layers per decade of pressure, with a linear-in- τ approximation for the variation of the source function within each layer. A 5-stream Gaussian quadrature grid in the emission angle cosine was used to integrate the disk-averaged flux. Tests confirmed that the cloud opacities derived for Saturn, even for large ($\lambda > 1 \mu\text{m}$) particles (*e.g.* Orton 1983) did not exert a significant influence on the upwelling radiance. Atmospheric opacities for this model are given in detail below.

Part of the continuum opacity of Saturn's infrared spectrum arises from the collision-induced dipole of H_2 , as influenced by H_2 and He collisions. The collision-induced opacity was modeled following Birnbaum *et al.* (1996). The mixing ratios of H_2 and He were assumed to be 96% and 4%, respectively (Conrath *et al.* 1984).

A detailed, line-by-line code was used to integrate over discrete molecular transitions. Transition frequencies, line strengths and ground state energies for these molecules were taken from the spectral line catalog of Pickett *et al.* (1992). The line widths for NH_3 pressure-broadened by H_2 and their temperature dependences were taken from Brown and Peterson (1994) and reduced by 10% as an approximation to the influence of He broadening. The shape of NH_3 inversion lines broadened by H_2 were modeled using the "modified Ben-Reuven" form derived by Berge and Gulikis (1976), with the modifications proposed by Joiner and Steffes (1991). The shape of the rotational NH_3 lines broadened by H_2 was modeled using the line coupling derived by Birnbaum *et al.* (1999). The pressure-broadened line widths for PH_3 broadened by H_2 and He were taken from a general formula given by Levy *et al.* (1993), their temperature dependence was taken from Levy *et al.* (1994), and VanVleck-Weiskoff lineshapes were assumed.

The disk-averaged temperature profile was taken from the Infrared Space Observatory Short-Wavelength Spectrometer investigation of Saturn's disk-averaged structure and composition (*e.g.* Bézard *et al.* 1998), kindly supplied by Bruno Bézard (Fig. 2). This profile was chosen over earlier ones as it averaged over the entire disk, similar to our observations, rather than being applicable

to a specific region or regions of the planet, such as the Voyager IRIS experiments (*e. g.* Conrath and Pirraglia 1983) or the Voyager radio occultation experiment (Lindal *et al.* 1987).

The mixing ratio of NH_3 below total pressures of about 1 bar (temperatures less than 135 K) is taken to be the saturated mixing ratio above the ammonia condensation level, consistent with various studies in the thermal infrared (*e.g.* Courtin *et al.* 1984). However at higher pressures and temperatures, and deeper than the condensation level, the abundance is a significant opacity source for the ~ 280 GHz spectral region. Because of the difficulty of sounding this region through cloud cover in the infrared, NH_3 abundances have been determined from the submillimeter through radio spectrum. The NH_3 mixing ratio profile has been given by (i) dePater and Massie (1985) as 5×10^{-4} for $p > 3$ bar and 3×10^{-5} for $p < 1.25$ bar, (ii) Briggs and Sackett (1989) as $4 - 6 \times 10^{-4}$ for $p \sim 25$ bar and decreasing to $0.7 - 1.1 \times 10^{-4}$ for $p \sim 2$ bars, and (iii) Grossman *et al.* (1989) as 1.2×10^{-4} just below the condensation level. We therefore selected a nominal mixing ratio of 1×10^{-4} below the condensation level.

We tested the sensitivity of the spectrum to the uncertainty of the value of the deep NH_3 mixing ratio, using a lower value of 3×10^{-5} and an upper value of 4×10^{-4} . The only effect on the spectrum was to vary the continuum brightness temperature far from the PH_3 1-0 line by less than ± 2 K. We note that the continuum far from the PH_3 3-2 line is influenced neither by variations of the PH_3 nor of the NH_3 mixing ratios in the deep atmosphere. Therefore, the only consequence of changing the NH_3 mixing ratio in the deep atmosphere is to change the continuum level in the 280-GHz region away from its observed levels. We retain the nominal deep NH_3 mixing ratio of 1×10^{-4} , understanding that the value is uncertain by factors of $\sim 3 - 4$, but that the nominal value is reasonably consistent with the independently measured continuum radiances in the 280-GHz region discussed earlier.

PH_3 Models

Originally the 1-0 PH_3 line was fit by a constant tropospheric mixing ratio of 3×10^{-6} and a stratospheric cutoff (Weisstein and Serabyn 1994). Figures 1 and 2 illustrate several models with a constant tropospheric mixing ratio with a stratospheric cutoff. A lower value for this mixing

ratio provides profiles that are narrower than both the observed lines. Higher values yield a profile that is wider than the 3-2 line. However, while a value of 3×10^{-6} fits both lines best, it is both narrower and deeper than the observed the 1-0 line. In fact, the primary observations indicate very different widths for the two lines: 10 GHz at 267 GHz *vs* 25-30 GHz at 805 GHz. Thus, a single mixing ratio is probably inappropriate to fit both lines simultaneously.

These models cut off the PH₃ distribution just above the 100-mbar level, allowing no emission to arise from the thermally “inverted” hot stratosphere. Figure 1 shows that, as a result, no emission core appears at the center of the strong 3-2 line. In fact, making this assumption, the brightness temperature of Saturn at this line center is controlled only by the assumed value of the temperature minimum. On the other hand, the high-frequency brightness temperatures in the continuum are dominated by H₂ opacity and change little with variations of the PH₃ mixing ratio. Thus, they are also generally fixed by the choice of the temperature profile. Thus, the radiance of the 800-GHz spectrum is fixed by the choice of the temperature structure in two ways, matching the brightness temperature of the line center, and of the distant continuum. It turns out that a single scaling of our spectrum matches both quantities fairly well. The reasonable agreement between the models and the data both at the center of the line, as well as in the distant line wings, thus attests to the general appropriateness of the chosen temperature structure, as well as to the accuracy of the fundamental measured quantity, the line to continuum ratio.

Since the 1-0 line arises from deeper levels than the 3-2 line, a better model would decrease the PH₃ mixing ratio with altitude. In fact, we can adopt a model in which the mixing ratio varies continuously as a function of pressure throughout the entire vertical range to which our measurements are sensitive, using a linear relationship between the logarithm of the mixing ratio and the logarithm of the pressure. This model is shown as the solid line in Fig. 3, and the mixing ratio in this relationship can be expressed as a power law in pressure: $3.2 \times 10^{-10} p^{1.55}$, for p in mbar. This model is the result of a least-squares fit to the data that define the lines. The fit of this model to the data is shown in Fig. 4.

Fig. 3

Fig. 4

The sensitivity of the model to the level of the upper tropospheric cutoff is also illustrated in

Figs. 3 and 4. Clearly the cutoff must be at a pressure lower than 250 mbar (alternating dashed-dotted line), which produces a spectrum whose 3-2 line is much shallower than observed. A cutoff at 160 mbar (short dashed line) produces a not unreasonable fit to the 3-2 line. A cutoff at 100 mbar (dotted line) shows no significant differences from the spectrum produced by the continuous curve (solid line), nor are models with cutoffs applied at even lower pressures. Because of the assumed rapid vertical falloff, the mixing ratio in the warm stratosphere is insufficient to produce an “inversion core” at the center of the 3-2 line. We will adopt this continuous model (solid line) profile as our nominal model, using the relationship given above to define the PH_3 mixing ratio for all pressures down to 10 mbar.

This simple model does not provide perfect fits to both spectral regions simultaneously. In fact, there is a direct tradeoff between the quality of the fit to the spectrum at the 1-0 line and in the wings of the 3-2 line. A larger mixing ratio near the 200-mbar level (temperatures near 110 K) would produce a better fit to the PH_3 1-0 line, but it would make the fit to the 3-2 line worse in the 812 - 828 GHz region. The proximity of the vertical sensitivities of these two regions is illustrated in Fig. 5 which shows the weighting functions associated with the outgoing radiances in the center and mid-wings of the two lines. The radiance at 267 GHz and at 812 and 818 GHz arise from pressures of 200 to 300 mbar. Nevertheless, limitations in these initial observations, such as the subtracted sine wave ripple in the 1-0 line and the low transmission below ~ 790 GHz, make these models acceptable at this point. Our inability to provide a perfect fit to both spectral regions simultaneously, together with the level of random noise, result in an uncertainty of some 25% in the value of the mixing ratio. The uncertainty of the molecular spectroscopic data has less than a 2% effect on the derived value for the PH_3 mixing ratio.

Fig. 5

We note that, as discussed above, the uncertainty of NH_3 mixing ratio produces an uncertainty in the continuum around the 1-0 line. This would require an overall rescaling of the brightness of the 240 - 300 GHz spectrum. Such a change would require a 20% adjustment in the PH_3 mixing ratio in the 400-700 mbar pressure range, and that must be considered a source of systematic uncertainty.

Fig. 5 also illustrates the range of depths to which we are sensitive, approximately 100 to 600 mbar. The 1-0 line, in particular, is a very good probe for the PH₃ abundance at depth. Note that even higher J rotational lines of PH₃ will arise from higher in the atmosphere than even the 3-2 line and will, therefore, be sensitive to the mixing ratio of PH₃ near the 150-mbar level. It is thus the lowest 1-0 line that provides us with information from deepest in the atmosphere.

Figs. 3 and 4 also illustrate the effect of modifying the simple best fit model distribution at depth. Adopting a constant mixing ratio for pressures of 1 bar and greater (not shown), as expected, does not produce any significant change to the model. Adopting a constant mixing ratio for pressures of 630 mbar or greater (long-dashed line) produces brighter radiances in the wings of the 1-0 line, and hence a somewhat better overall fit to the data. On the other hand, a model with a constant mixing ratio for pressures greater than 400 mbar (dashed-triple-dotted line) produces a PH₃ 1-0 line that is clearly narrower than observed (Fig. 4). We thus adopt the model with a linear dropoff of $\log(\text{PH}_3)$ vs $\log(\text{pressure})$ and a constant mixing ratio for pressures greater than 630 mbar as our standard model for the remainder of this paper. The value at 630 mbar (1.2×10^{-5}) then serves as a reasonable estimate of the value for the PH₃ mixing ratio at depth. If the mixing ratio increases at pressures greater than 630 mbar, then this number represents a hard constraint for the minimum value.

We undertook to improve the model by inverting the spectral data and solving for the abundance of PH₃ as a function of depth between 100 and 630 mbar, using the generalized remote sensing inversion approach of Chahine (1970) and the nominal model as an initial guess. The results, in fact, were not significantly different from those of the nominal model, and only a 25% improvement in the residuals to the data was achieved.

We also checked the results after perturbing the temperature structure. If the temperature profile is lowered uniformly by 2 K, the spectrum can then be fit by lowering the PH₃ mixing ratio by 25% uniformly (Fig. 6). The results are, in fact, slightly better than the standard model at the center of the 3-2 line, but otherwise not significantly different from it. Fig. 6

Finally, we point out that, while two transitions of HCN are within our spectral range (265.8

and 797.4 GHz), tests show that they would be detectable above our noise level only if the upper tropospheric mixing ratios were greater than or equal to 3×10^{-9} . That is significantly higher than the upper limit of the HCN mixing ratio of 4×10^{-10} derived by Weisstein and Serabyn (1996) on the basis of other non-blended HCN line positions.

Comparison with Other Results

Our standard model for the global average of the vertical distribution of PH_3 in Saturn is shown in Fig. 7, with the solid line highlighting the approximate vertical range to which we are sensitive. We are insensitive to the PH_3 abundance at atmospheric pressures below ~ 100 mbar because of the isothermal nature of the temperature structure. The steep linear dropoff of our model does not create an emission core in the 3-2 PH_3 line. Furthermore, it is consistent with the low PH_3 abundance required by Winkelstein *et al.* (1983) above the 25-mbar level in order to match Saturn's 180 - 220 nm spectrum. The profile is a bit higher than the PH_3 mixing ratio upper limits derived from Hubble Space Telescope Faint-Object Spectrograph ultraviolet data for latitudes at and poleward of 36°N (Edgington *et al.* 1998), and it is possible that our whole-disk observations are dominated by the signatures of the PH_3 vertical profile for low-latitude regions. We are generally insensitive to the PH_3 abundance at pressures much above ~ 630 mbar, but we find that a constant mixing ratio with depth is more consistent with the data than an extrapolation of steep increase that holds at lower pressures.

Fig. 7

The PH_3 vertical distribution derived by Courtin *et al.* (1984) (Fig. 7) is not consistent with our data. Similar to all models with a constant mixing ratio in the troposphere (*e.g.* Tokunaga *et al.* 1980, 1981), it cannot fit both our observed lines simultaneously. Furthermore, its constant PH_3 mixing ratio of 1.45×10^{-6} up to the 3-mbar level (where the stratospheric temperature is ~ 130 K in our model) produces an unmistakable emission core that is well above our noise level (Fig. 8).

Fig. 8

The PH_3 distribution used to model the ISO/SWS middle-infrared spectrum of Saturn (de-Graauw *et al.* 1997) is also shown in Fig. 7. It is not distributed uniformly in the troposphere, but the mixing ratio is generally too low to fit either of the 1-0 or 3-2 lines (Fig. 8).

Noll and Larson's (1990) vertical distribution was the only nonuniform tropospheric vertical distribution of PH_3 based on measurement constraints in the literature prior to the ISO mission. While employing a simple stepfunction at the 400-mbar level, it nevertheless appears close to the values in our smoother distribution (Fig. 9), and its spectrum does reasonably well at matching our 3-2 observations. Furthermore, changing the location of the step to the 500-mbar level, and increasing the value of the deeper mixing ratio from 7×10^{-6} to 2.2×10^{-5} , achieves a fit to both lines that is generally as good as our nominal model (Fig. 10).

One of the main conclusions of our work is that the deep atmospheric mixing ratio of PH_3 must be at least 1×10^{-5} . The value could also be higher. Our data do not constrain well the mixing ratio deeper than the ~ 700 -mbar level, and a further increase with depth could be consistent with our data. This deep PH_3 mixing ratio implies a $[\text{P}]/[\text{H}]$ abundance ratio that is at least 10 times the one expected from the solar ratio, consistent with Noll and Larson's (1990) results.

Chemical and Transport Models

It also appears both from our data and from the $5\text{-}\mu\text{m}$ spectrum of Saturn, that the PH_3 vertical distribution drops sharply with altitude in the upper troposphere of Saturn. The question that then arises is the origin of this effect: given that Saturn is too warm for PH_3 condensation, is the dropoff the result of increased chemical scavenging with height, disequilibrium tropospheric chemistry, or photodissociation?

Qualitatively, the dropoff has the morphology of the vertical distribution of NH_3 in Jupiter for pressures less than 8 bars at the Galileo probe entry site as determined by the attenuation of the probe relay antenna (Folkner *et al.* 1998). However, unlike PH_3 , NH_3 is a condensate in both Jupiter and Saturn, and it is also subject to chemical scavenging by H_2S . In addition, the Galileo probe entered the atmosphere in an unusually clear and possibly dry, downwelling region (Orton *et al.* 1998) that may not be at all characteristic of the average conditions on the planet. In fact, in the absence of H_2O , which is expected to condense at pressures of several bars (*e.g.* Prinn *et al.* 1984, there are few established theoretical reasons to support any specific chemical mechanisms for removing PH_3 from Saturn's atmosphere that are effective at the atmospheric levels in question.

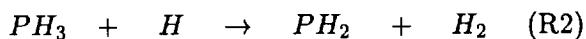
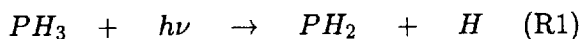
The tropospheric chemistry of PH_3 has been modeled by Prinn *et al.* (1984), Prinn and Fegley (1985) and Fegley and Lodders (1994). All of the models show that PH_3 is subject to a reaction with H_2O to form P_4O_6 and molecular hydrogen. For conditions of thermochemical equilibrium, at the temperatures to which our spectra are sensitive, the mixing ratio of PH_3 should be orders of magnitude lower than detected, with the reaction favoring P_4O_6 below temperatures of about 950 K. For temperatures below 404 K, condensation of $\text{CH}_4\text{H}_2\text{PO}_4(\text{s})$ decreases the abundance of gaseous P_4O_6 (*cf.* Fig. 3 of Fegley and Prinn, 1985). The timescale for establishing equilibrium chemistry, therefore, must be much longer than the timescale for vertical mixing. The temperature at the level where chemical equilibration takes place at a rate equal to the vertical mixing rate is known as the “quench temperature”, estimated by Prinn *et al.* as close to 1200 K. Above this level in Saturn, the vertical mixing is sufficiently rapid that the mixing ratio of PH_3 remains essentially constant. Fig. 33 of Fegley and Lodders (1994), plots the PH_3 mixing ratio expected to be observable in the upper troposphere *vs* the vertical eddy diffusion coefficient. It is possible, of course, to envision that the time scale for vertical mixing increases dramatically toward the tropopause, together with the static stability of the atmosphere against buoyancy. However, even if we required the vertical mixing of PH_3 to slow down in order to accommodate destruction by H_2O , it would not take place in the region to which we are sensitive, which is well above the condensation level for H_2O (several bars of pressure). The extremely low observed mixing ratio of H_2O (de Graauw *et al.* 1997) makes the efficacy of PH_3 oxidation reactions in the 100 - 800 mbar range an unlikely cause for its depletion.

The alternative is, of course, photochemical destruction of PH_3 . To test the photochemical removal of PH_3 in the upper troposphere, and the impact of varying vertical motion in this region, we used the Caltech/JPL 1-D photochemical model (Allen *et al.* 1981) to solve photochemical reactions and dynamical transport of PH_3 and other relevant species in each pressure level. This model incorporated PH_3 and NH_3 photochemical reactions, molecular and bulk atmospheric vertical motions, condensation of NH_3 below the tropopause, and the attenuation of solar radiation by absorption and scattering. The reactions used in the model are listed in Table 1.

Several more reactions involving NH_3 and related molecules were included originally, but their

removal was found to make a negligible change in the model results. Because the region of interest is well above the NH_3 saturation level, its partial pressure is no greater than the saturation vapor pressure. As a result, the NH_3 mixing ratio ($\sim 10^{-8}$ at 500 mbars pressure) is too low to affect the model results. Turning off all nitrogen-related chemistry produces negligible changes in the abundance or distribution of PH_3 in our model. We did retain the direct photolysis of NH_3 in the model, although the small number of H atoms that are produced by direct NH_3 photolysis turned out to be too low to be of any consequence in the results. We retained the reaction involving scavenging of PH_3 by NH_2 to illustrate quantitatively its minimal importance in the chemistry. We also explicitly modeled NH_3 absorption in the spectrum, although it turned out that NH_3 shielding of the UV spectrum was negligible.

There are three photochemical reactions that can remove PH_3 by decomposition in this model:



The loss rate profiles for each of these reactions are compared in Fig. 11. The attack of PH_3 by NH_2 radicals (reaction R3) is not as important as reactions R1 and R2 because only very small amounts of NH_3 are present in this part of Saturn's atmosphere. PH_3 loss from photolysis and from attack by H atoms are nearly equal everywhere near the tropopause, because the primary source of the H atoms (reaction R2) is, in fact, PH_3 photolysis itself (reaction R1). Fig. 11

The primary sources of error in our photochemical model results could thus be attributed to uncertainties in the R1 reaction from the photolysis cross-section, or in the R2 reaction. Uncertainties in the R2 reaction, stemming from the $\sim 15\%$ uncertainty of the rate constant (Arthur *et al.* 1997), propagate into a mere 10% uncertainty of the best-fit eddy diffusion coefficient (see below). On the other hand, uncertainties in the R1 reaction influence both the direct photolysis of PH_3 and the production of H atoms. Thus, it is the primary source of uncertainty for the R2 reaction because it

is the primary source of H atoms in the part of the atmosphere under study. Our testing shows that perturbations of the PH_3 cross-section (Chen *et al.* 1991) transfer proportionally into the derived values of the eddy diffusion coefficient. Unfortunately, Chen *et al.* do not quote an uncertainty associated with their observations. More realistically, it is likely that the largest contribution to the uncertainty is derived from the extension of their low-temperature (155 K) measurements to wavelengths greater than 2100 Å. This extension is important to our work, because there are many more solar photons available between 2100 Å and the photodissociation limit at 2300 Å than at shorter wavelengths, even though the cross-section spectrum itself is much weaker than at shorter wavelengths. Simulating the worst case, if the cross-section is set to zero for wavelengths longward of 2100 Å, there is only a 30% drop of the derived value of the eddy diffusion coefficient. This test includes both the loss of PH_3 through a diminished photolysis (R1) and through a diminished population of scavenging H atoms (R2).

The abundance of PH_3 is sensitive to vertical motion in the upper troposphere, as pointed out by Kaye and Strobel (1984). The characteristic vertical motion is conventionally parameterized by means of the eddy diffusion coefficient, which corresponds to macroscopic bulk atmospheric vertical motion. Prinn *et al.* (1984) note that uniform values for the eddy diffusion coefficient are expected for the troposphere for either free convection or baroclinic eddies, with values in the range of 10^7 to $10^9 \text{ cm}^2 \text{ sec}^{-1}$. If these large values are applied over the vertical range to which our data are sensitive, our models predict little deviation from a uniform mixing ratio, which is in conflict with our best fitting model.

In a more realistic modeling approach, we held the mixing ratio constant for pressures greater than 630 mbar, corresponding to the vigorous mixing associated with the troposphere, and tested smaller values for pressures less than 630 mbar, similar to the models of Kaye and Strobel (1984). In fact, the 630-mbar level is close to the radiative-convective boundaries at various latitudes in the spatially-resolved time-dependent radiative-convective models of Bézard *et al.* (1984). Vertical transport above this level is likely to be dominated by upwelling waves, which are stable only in the radiative part of the atmosphere (*e.g.* Lindzen 1971, for the earth's atmosphere). Consistent

with this model, we held the value of the mixing ratio constant at 630 mbar and assumed various values for the eddy diffusion coefficient at this level, varying it above this point according to the inverse of the atmospheric density. The inverse-density variation is appropriate for transport by vertically propagating non-dissipative waves (Strobel 1981) and yields a better fit to our data than an inverse-square-root dependence on the atmospheric density, another popular assumption *e.g.* Prinn *et al* 1984). Both the PH₃ mixing ratio and the eddy diffusion coefficient at the 630-mbar level were varied in order to optimize the fit to the data. These results are shown in Fig. 12 with the corresponding spectra shown in Fig. 13. While none of the models provides as good a fit as to the spectrum as our standard model, the best model (dash-dotted curves) does provide reasonable agreement. This model has an eddy diffusion coefficient at 630 mbar of $\sim 10^4$ cm² sec⁻¹, with a conservative estimate of the uncertainty as about a factor of two, and increases by some 50% over the region to which we are sensitive.

Fig. 12
Fig. 13

The fact that the best models are consistent with an increase in the eddy diffusion coefficient taking place immediately above the radiative-convective boundary implies that upward propagating waves are also present immediately above this boundary. This is consistent with their presence just above the radiative-convective boundary in Jupiter's atmosphere, as well, as indicated by the thermal oscillations measured by the Galileo Probe Atmospheric Structure instrument (Seiff *et al.* 1998).

Our values for the eddy diffusion coefficient near Saturn's tropopause, close to the top of the region to which we are sensitive, are ostensibly some two orders of magnitude higher than those given by Moses *et al.* in their analysis of stratospheric hydrocarbon photochemistry at the same pressure level. However, their models are not really sensitive to values of the eddy diffusion coefficient for pressures higher than 50 mbar, so long as they drop to values less than 10^3 cm² sec⁻¹ somewhere in the 10 - 60 mbar region (J. Moses, pers. comm.). Thus, we expect that the profile of the eddy diffusion coefficient drops from a high value $\sim 10^7 - 10^8$ cm² sec⁻¹ in the troposphere (Prinn *et al.* 1984) for pressures greater than ~ 700 mbar, to a value near 10^4 cm² sec⁻¹ that we derive here for the radiative-convective boundary near 630 mbar, increases again with altitude through pressures

of 150 mbar or lower, then drops further above the 100-mbar level to values near $10^3 \text{ cm}^2 \text{ sec}^{-1}$ as required by the hydrocarbon models of Moses *et al.* (1999).

We expect that continuing work in regions of the infrared that are dominated by strong PH_3 absorption would help to confirm and extend upward our determination of the abundance of PH_3 closer to the level of the temperature minimum, near 100 mbar pressure. Spatially resolved observations would also help to determine the dependence of the PH_3 mixing ratio on local variations of the vertical wind regime, particularly if correlations with the abundances of local NH_3 condensate particles could be established. Edgington *et al.* (1998) noted that there were latitudinal variations of the maximum PH_3 mixing ratio in the lower stratosphere allowed by models of their ultraviolet spectra, with the trend being that lower latitudes exhibited higher abundance upper limits for PH_3 . In theory, extending spatially dependent studies of the PH_3 mixing ratio deeper into the atmosphere could be done at an even drier site using a wide-band, high-resolution spectrometer that covers the PH_3 3-2 and 1-0 submillimeter lines and spatial resolution that resolves major banded features on Saturn, such as the envisioned Atacama Large Millimeter Array. The spectra from such an instrument would constrain models for the vertical wind regime of the atmosphere as a function of latitude. Until such an instrument is deployed, however, we can use techniques that detect both moderate and weak PH_3 lines at shorter wavelengths, even without resolving the individual line shapes, coupled with appropriate cloud models from accurate continuum measurements. Such observations are planned by both the Cassini Visible and Infrared Mapping Spectrometer (VIMS) and the Composite Infrared Spectrometer (CIRS) experiments, although they will not be sensitive to PH_3 distributed as deep as 600 mbar. However, only direct probes of Saturn's atmosphere are likely to be successful in elucidating the PH_3 mixing ratio for pressures much greater than 600 mbar.

Acknowledgements

We are grateful for helpful discussions with Mark Allen, Sushil Atreya, Linda Brown, Gordon Bjoraker, Ed Cohen, Julie Moses and Darrell Strobel. We thank Bruno Bézard for a digital version of his disk-averaged temperature profile for Saturn that was derived from ISO/SWS data. We

also appreciate useful and illuminating comments from reviewers Scott Edgington and Paul Romani. A portion of this work was performed through the auspices of Jet Propulsion Laboratory Supercomputing Project Office. This work was supported by research grants to the Jet Propulsion Laboratory and the California Institute of Technology from the Planetary Astronomy and Planetary Atmospheres disciplines of the Office of Space Science and Applications of the National Aeronautics and Space Administration.

References

- Allen, M. Y. L. Yung, and J. W. Waters. 1981. Vertical transport and photochemistry in the terrestrial mesosphere and lower thermosphere (50-120 km). *J. Geophys. Res.* **86**, 3617 - 3627.
- Arthur, N. L. and I. A. Cooper. 1997. Arrhenius parameters for the reactions of H atoms with PH₃ and AsH₃. *J. Chem. Soc. Faraday Trans.* **93**, 521 - 524.
- Baulch, D. L., C. J. Cobos, R. A. Cox, C. Esser, P. Frank, Th. Just, J. A. Kerr, M. J. Pilling, J. Troe, R. W. Walker, and J. Warnatz. 1992. Evaluated kinetic data for combustion modeling. *J. Phys. Chem. Ref. Data* **21**, 411 - 734.
- Berge, G. L. and S. Gulkis. 1976. Earth-based radio observations of Jupiter: Millimeter to meter wavelengths. In *Jupiter*, T. Gehrels, Ed. Univ. of Arizona Press, Tucson. pp. 621-692.
- Bézard, B., D. Gautier, and B. Conrath. 1984. A seasonal model of the Saturnian upper troposphere: Comparison with Voyager infrared measurements. *Icarus* —*bf* **60**, 274 - 288.
- Bézard, B., H. Feuchtgruber, J. I. Moses, and T. Encrenaz. 1998. Detection of methyl radicals (CH₃) on Saturn. *Astron Astrophys.* **334**, L41 - L44.
- Birnbaum, G., A. Borysow, and G. S. Orton. 1996. Collision-induced absorption of H₂-H₂ and H₂-He in the rotational and fundamental band for planetary applications. *Icarus* **123**, 4 - 22.
- Birnbaum, G., A. Buechele, T. Jian, G. S. Orton, Z. Hadzibabic, and G. R. John. 1999. Absorption in the troughs of the far infrared spectra of NH₃ and mixtures of NH₃ and H₂. *J. Quant. Spectrosc. Radiat. Transf.* In press.
- Borunov, S., V. Dorofeeva, I. Chodakovsky, P. Drossart, E. Lellouch, and T. Encrenaz. 1995. Phosphorus chemistry in the atmosphere of Jupiter: A reassessment. *Icarus* **113**, 460 - 464.
- Bosco, S. R., W. D. Brobst, D. F. Nava, L. J. Stief. 1983. The reaction NH₂ + PH₃ → NH₃ + PH₂: Absolute rate constant measurement and implication for NH₃ and PH₃ photochemistry in the atmosphere of Jupiter. *J. Geophys. Res.* **88**, 8543 - 8549.
- Bregman, J. D., D. F. Fester, and D. M. Rank 1985. Observation of the ν₂ band of PH₃ in the atmosphere of Saturn. *Astrophys. J. Lett.* **202**, L55 - L56.
- Briggs, F. H. and P. D. Sackett. 1989. Radio observations of Saturn as a probe of its atmosphere

and cloud structure. *Icarus* **80**, 77-103.

Brown, L. R. and D. B. Peterson. 1994. An empirical expression for linewidths of ammonia from far-infrared measurements. *J. Molec. Spectrosc* **168**, 593 - 606.

Chahine, M. T. 1970. Inverse problems in radiative transfer: Determination of atmospheric parameters. *J. Atmos. Sci* **27**, 960 - 967.

Chen, F., D. L. Judge, R. C. Y. Wu, J. Caldwell, P. White, and R. Wagener, 1991. High-resolution, low-temperature photoabsorption cross sections of C₂H₂, PH₃, AsH₃, and GeH₄, with application to Saturn's atmosphere. *J. Geophys. Res.* **96**, 17519 - 17527.

Conrath, B. J. and J. A. Pirraglia. 1983. Thermal structure of Saturn from Voyager infrared measurements: Implications for atmospheric dynamics. *Icarus* **53**, 286-292.

Conrath, B. J. D. Gautier, R. A. Hanel, and J. S. Hornstein. 1984. The helium abundance of Saturn from Voyager measurements. *Astrophys. J.* **282**, 807 - 815.

Courtin, R. N. Coron, T. Encrenaz, R. Gispert, P. Bruston, J. Leblanc, G. Dambier, and A. Vidal-Madjar. 1977. Observations of giant planets at 1.4 mm and consequences on the effective temperatures *Astron. Astrophys.* **60**, 115 - 123.

Courtin, R., D. Gautier, A. Marten and B. Bézard. 1984. The composition of Saturn's atmosphere at northern temperate latitudes from Voyager IRIS spectra: NH₃, PH₃, C₂H₂, C₂H₆, CH₃D, CH₄. *Astrophys. J.* **287**, 899 - 916.

Davis, G. R., M. J. Griffin, D. A. Naylor, P. G. Oldham, B. M. Swinyard, P. A. R. Ade, S. B. Calcutt, T. Encrenaz, T. de Graauw, D. Gautier, P. G. J. Irwin, E. Lellouch, G. S. Orton, C. Armand, M. Burgdorf, A. DiGiorgio, D. Ewart, C. Gry, K. J. King, T. Lim, S. Molinari, M. Price, S. Sidher, A. Smith, D. Texier, N. Trams, S. J. Unger. 1996. ISO LWS measurement of the far-infrared spectrum of Saturn. *Astron. Astrophys.* **315**, L393-396.

dePater, I. and S. T. Massie. 1985. Models of the millimeter-centimeter spectra of the giant planets. *Icarus* **62**, 143-171.

Edgington, S. G., S. K. Atreya, L. M. Trafton, J. J. Caldwell, R. F. Beebe, A. A. Simon, R. West and C. Barnet. 1998. Phosphine mixing ratios and eddy mixing coefficients in the troposphere of

Saturn. *Bull. Amer. Astron. Soc.* **29**, 992.

Fegley, B. and R. G. Prinn. 1985. Equilibrium and nonequilibrium chemistry of Saturn's atmosphere - Implications for the observability of PH₃, N₂, CO and GeH₄. *Astrophys. J.* **299**, 1067 - 1078.

Fegley, B., Jr. and K. Lodders. 1994. Chemical models of the deep atmospheres of Jupiter and Saturn. *Icarus* **110**, 117 - 154.

Fink, U. and H. P. Larson. 1977. The 5 μ spectrum of Saturn. *Bull. Amer. Astron. Soc.* **9**, 535.

Folkner, W. M., R. Woo., and S. Nandi. 1998. Ammonia abundance in Jupiter's atmosphere derived from the attenuation of the Galileo probe's radio signal. *J. Geophys. Res.* **103**, 22,847 - 22,855.

Gillett, F. C and W. J. Forrest. 1974. *Astrophys. J. Lett.* **187**, L39.

Grossman, A. W., D. O. Muhleman and G. L. Berge. 1989. High-resolution microwave images of Saturn. *Science* **245**, 1211-1215.

De Graauw, T., H. Feuchtgruber, B. Bézard, P. Drossart, T. Encrenaz, D. A. Beintema, M. Griffin, A. Heras, M. Kessler, K. Leech, E. Lellouch, P. Morris, P. R. Roelfsema, M. Roos-Serote, A. Salama, B. Vandenbussche, E. A. Valentijn, G. R. Davis, and D. A. Naylor. 1997. First results of ISO-SWS observations of Saturn: Detection of CO₂, CH₃H₂H, C₄H₂ and tropospheric H₂O. *Astron. Astrophys.* **321**, L13 - L16.

Feuchtgruber, H., E. Lellouch, T. de Graauw, B. Bézard, T. Encrenaz, and M. Griffin. 1997. *Nature* **389**, 159 - 162.

Ham, D. O., D. W. Trainor, and F. Kaufman. 1970. Gas phase kinetics of $H + H + H_2 \rightarrow 2H_2$. *J. Phys. Chem.* **53**, 4395 - 4396.

Husain, D., and P. E. Norris. 1977. Reactions of phosphorus atoms, P(34S3/2), studied by attenuation of atomic resonance radiation in the vacuum ultraviolet. *J. Chem. Soc. Faraday Trans 2* **73**, 1107 - 1115.

Joiner, J. and P. G. Steffes. 1991. Modeling of Jupiter's millimeter wave emission utilizing

laboratory measurements of ammonia (NH₃) opacity. *J. Geophys. Res.* **96**, 17463 - 17470.

Kaye, J. A. and D. F. Strobel. 1984. Phosphine photochemistry in the atmosphere of Saturn. *Icarus* **59**, 314 - 335.

Lindzen, R. S. 1971. Tides and gravity waves in the upper atmosphere. In *Mesospheric models and related experiments* (G. Fiocco, Ed.), pp. 122 - 130, D. Reidel, Boston.

Lee, J. H., J. V. Michael, W. A. Payne, D. A. Whystock, L. J. Stief. 1976. Absolute rate constant for the reaction of atomic hydrogen with phosphine over the temperature range 209 to 495 K. *J. Chem. Phys.* **65**, 3280 - 3283.

Leroy, G., M. Sana, and A. Tinant, 1985, Etude theorique des reactions d'abstraction d'hydrogene $RH + X = R + HX$, avec R, X≡H, CH₃, NH₂, OH et F. *Can. J. Chem.* **63**, 1447 - 1456.

Levy, A., N. Lacombe, and G. Tarrago. 1993. Hydrogen-broadening and helium-broadening of phosphine lines. *J. Molec. Spectrosc.* **157**, 172 - 181.

Levy, A., N. Lacombe, and G. Tarrago. 1994. Temperature-dependence of collision-broadened lines of phosphine. *J. Molec. Spectrosc.* **166**, 20 - 31.

Lindal, G. F., D. N. Sweetnam, and V. R. Eshleman. 1985. The atmosphere of Saturn: An analysis of the Voyager radio occultation measurements. *Astron. J.* **90**, 1136 - 1146.

Moses, J. I., G. R. Gladstone, H. Feuchtgruber, and M. Allen, 1999. Photochemistry of the upper atmosphere of Saturn. I. Hydrocarbon chemistry and comparisons with ISO Observations. *Icarus*. In press.

Noll, K. S. and H. P. Larson. 1990. The spectrum of Saturn from 1990 to 2230 cm⁻¹: Abundances of AsH₃, CH₃D, CO, GeH₄, NH₃ and PH₃. *Icarus* **89**, 168 - 189.

Orton, G. 1983. Thermal infrared constraints on ammonia ice particles as candidates for clouds in the atmosphere of Saturn. *Icarus* **53**, 293 - 300.

Orton, G. S., B. M. Fisher, S. T. Stewart, A. J. Friedson, J. L. Ortiz, M. Marinova, W. Hoffmann, J. Hora, M. Ressler, S. Hinkley, V. Krishnan, M. Masanovic, J. Tesic, A. Tziolas, and K. Parija. 1998. The Galileo Probe entry site: Characteristics of the Galileo Probe entry site from earth-based remote sensing observations. *J. Geophys. Res.* **103**, 22,791 - 22,814.

Pickett, H. M., R. L. Poynter, and E. A. Cohen. 1992. Submillimeter, millimeter, and microwave spectral line catalogue. JPL Publ. 80-23, Rev. 3, Jet Propulsion Laboratory, Pasadena, California.

Prinn, R. G., H. P. Larson, J. J. Caldwell, and D. Gautier. 1984. Composition and chemistry of Saturn's atmosphere. In *Saturn* (T. Gehrels and M. S. Matthews, Eds.), pp. 88-149. Univ. of Arizona Press. Tucson.

Roellig, T. L., M. W. Werner, and E. E. Becklin. 1988. Thermal emission from Saturn's rings at 380 μm . *Icarus* **73**, 574 - 583.

Roose, T. R., R. K. Hanson, and C. H. Kruger. 1978. Decomposition of NO in the Presence of NH_3 . *Symp. Int. Shock Tubes Waves Proc.* **11**, 245.

Seiff, A., D. B. Kirk, T. C. D. Knight, R. E. Young, J. D. Mihalov, L. A. Young, F. S. Milos, G. Schubert, R. C. Blanchard, D. Atkinson. 1998. Thermal structure of Jupiter's atmosphere near the edge of a 5- μm hot spot in the north equatorial belt. *J. Geophys. Res.* **103**, 22857 - 22889.

Stief, L. J., and W. A. Payne. 1976. Absolute rate parameter for the reaction of hydrogen with hydrazine. *J. Chem. Phys.* **64**, 4892 - 4896.

Strobel, D. F. 1981. Parameterization of linear wave chemical transport in planetary atmospheres by eddy diffusion. *J. Geophys. Res.* **86**, 9806 - 9810.

Tokunaga, A. T., H. L. Dinerstein, D. F. Lester, and D. M. Rank. 1980. The phosphine abundance on Saturn derived from new 10-micrometer spectra. *Icarus* **42**, 79 - 85.

Tokunaga, A. T., H. L. Dinerstein, D. F. Lester, and D. M. Rank. 1981. Erratum: "The phosphine abundance on Saturn derived from new 10-micrometer spectra (*Icarus* **42**, 79 - 85, 1980)". *Icarus* **48**, 540.

Ulich, B. L., J. R. Dickel, and I. dePater. 1984. Planetary observations at a wavelength of 1.32 mm *Icarus* **60**, 590 - 598.

Weisstein, E. W. and E. Serabyn. 1994. Detection of the 267 GHz $J=1-0$ rotational transition of PH_3 in Saturn with a new Fourier transform spectrometer. *Icarus* **109**, 367 - 371.

Weisstein, E. W. and E. Serabyn. 1996. Submillimeter line search in Jupiter and Saturn. *Icarus* **123** **23**, 23 - 36.

Werner, M. W., G. Neugebauer, J. R. Houck and M. G. Hauser. 1980. One-millimeter brightness temperatures of the planets. *Icarus* **35**, 289 - 296.

West, R. A., D. F. Strobel, and M. G. Tomasko. 1986. Clouds, aerosols, and photochemistry in the Jovian atmosphere. *Icarus* **65**, 161 - 217.

Winkelstein, P., J. Caldwell, S. J. Kim, M. Combes, G. E. Hunt, and V. Moore. A determination of the composition of Saturnian stratosphere using IUE. 1983. *Icarus* **54**, 309 - 318.

Table 1: Photochemical Reactions used in the model

Reaction	Rate Constant ¹	Reference
$\text{NH}_3 + h\nu \rightarrow \text{NH}_2 + \text{H}$	J_1 (80 - 2300 A)	
$\text{N}_2\text{H}_4 + h\nu \rightarrow \text{N}_2\text{H}_3 + \text{H}$	J_2 (1210 - 2050 A)	
$\text{PH}_3 + h\nu \rightarrow \text{PH}_2 + \text{H}$	J_3 (60 - 2100 A) ²	
$\text{P}_2\text{H}_2 + h\nu \rightarrow \text{P}_2 + \text{H}_2$	J_4	
$\text{P}_2\text{H}_4 + h\nu \rightarrow \text{P}_2\text{H}_3 + \text{H}$	J_5	
$2\text{H} + \text{M} \rightarrow \text{H}_2 + \text{M}$	$k_0 = 2.70 \times 10^{-31} \text{ T}^{-0.6}$	Ham <i>et al.</i> (1970)
$\text{H} + \text{CH}_3 \rightarrow \text{CH}_4$	$k = 3.5 \times 10^{-10}$	Baulch <i>et al.</i> (1992)
$\text{P} + \text{H} + \text{M} \rightarrow \text{PH} + \text{M}$	$k_0 = 3.40 \times 10^{-33} e^{+173/T}$ $k_\infty = 2.00 \times 10^{-32}$	K.S.
$\text{P} + \text{H}_2 + \text{M} \rightarrow \text{PH} + \text{H} + \text{M}$	$k_0 = 5.00e10^{-15}$	Husain and Norris (1982)
$\text{P} + \text{PH} \rightarrow \text{P}_2 + \text{H}$	$k = 5.00 \times 10^{-11} e^{-400/T}$	K.S.
$2\text{P} + \text{M} \rightarrow \text{P}_2 + \text{M}$	$k_0 = 1.40 \times 10^{-33} e^{+500/T}$	K.S.
$\text{PH} + \text{H} \rightarrow \text{P} + \text{H}_2$	$k = 1.50 \times 10^{-10} e^{-416/T}$	K.S.
$\text{PH} + \text{H}_2 + \text{M} \rightarrow \text{PH}_3 + \text{M}$	$k_0 = 3.00 \times 10^{-36}$	K.S.
$2\text{PH} \rightarrow \text{P}_2 + \text{H}_2$	0	
$\text{PH}_2 + \text{H} \rightarrow \text{PH} + \text{H}_2$	$k = 6.20e10^{-11} e^{-318/T}$	K.S.
$\text{PH}_2 + \text{H} \rightarrow \text{PH}_3$	$k = 3.70e10^{-11} e^{-340/T}$	K.S.
$\text{PH}_2 + \text{CH}_3 \rightarrow \text{CH}_3\text{PH}_2$	$k = 1.20 \times 10^{-10} e^{-37/T}$	K.S.
$\text{PH}_2 + \text{NH}_2 \rightarrow \text{NH}_2\text{PH}_2$	$k = 1.00 \times 10^{-10} e^{-18/T}$	K.S.
$2\text{PH}_2 \rightarrow \text{P}_2\text{H}_4$	$k = 2.80 \times 10^{-11} e^{-30/T}$	K.S.
$\text{PH}_3 + \text{H} \rightarrow \text{PH}_2 + \text{H}_2$	$k = 7.21 \times 10^{-11} e^{-887/T}$	Arthur <i>et al.</i> (1997)
$\text{PH}_3 + \text{NH}_2 \rightarrow \text{PH}_2 + \text{NH}_3$	$k = 1.36 \times 10^{-12} e^{-984/T}$	Bosco <i>et al.</i> (1986)
$\text{P}_2 + \text{H} \rightarrow \text{PH} + \text{P}$	$k = 6.20 \times 10^{-11} e^{-318/T}$	

1 R0 - R5 are photodissociation rate constants in units of s^{-1} . Two-body rate constants are in units of $\text{cm}^3 \text{ molecule}^{-1} \text{ s}^{-1}$, and three-body rate constants are in units of $\text{cm}^6 \text{ molecule}^{-2} \text{ s}^{-1}$.

2 The value for R3 is for a diurnally averaged radiation field at 500 mbar, 10° N latitude, and PH_3 cross-sections for $\lambda \leq 1500 \text{ A}$ are taken from Chen *et al.* (1991), using a re-scaling of room-temperature results between 2100 and 2300 A.

3 K.S. represents Kaye and Strobel (1984)

FIGURE CAPTIONS

Figure 1. Brightness temperature spectra of Saturn's disk with normalization of radiances as described in the text. The sinusoid in the data between 240 and 250 GHz is an artifact of the data acquisition. Models with H₂ collision-induced opacity only are shown for reference with the alternating dotted-dashed line. Models with constant PH₃ mixing ratios in the troposphere below a rapid falloff near the 100-mbar level (Fig. 2) are shown by the three models indicated in the legend. The resolution of the spectra is approximately 200 MHz.

Figure 2. Vertical distribution of PH₃ for the models shown in Fig. 1, using the same line styles as the spectra. The temperature structure assumed is shown for reference by the dotted line.

Figure 3. Vertical distribution of PH₃ as in Fig. 2, but for a constant log mixing ratio *vs* log pressure relationship. Models that include stratospheric PH₃ cutoffs starting at 100, 160 and 250 mbars are shown by the dotted, short dashed, and dash-dotted lines, respectively. Models with deep tropospheric uniform mixing ratios starting at 630 mbar and 1 bar are shown by the triple-dotted-dashed and long dashed lines, respectively. We adopt the model given by the solid line as our nominal model. There is a $\pm 25\%$ uncertainty in the mixing ratio that arises from the noise and the remaining inconsistency between the two data sets.

Figure 4. Spectra of the models shown in Fig. 3, compared with our data, using the same linestyles as in Fig. 3.

Figure 5. Weighting functions of the outgoing radiance associated with the standard model shown by the solid line in Fig. 3 with the PH₃ cutoff pressure at 10 mbars. PH₃ 1-0 transition weighting functions are offset to the right arbitrarily and displayed by thicker lines for clarity. The secondary peaks are the result of the background continua arising from NH₃ line wing or H₂ collision-induced opacities.

Figure 6. Spectra of a perturbation of the standard model shown by the solid line in Fig. 3 with a temperature profile 2 Kelvins lower than the standard model and a PH₃ mixing ratio lower by 25% lower than the standard model. The spectrum of the standard model is displayed as the solid line, and the temperature perturbation is shown as the dashed line.

Figure 7. Vertical distributions of PH_3 . The standard model is given by the solid curve with thicker line indicating the vertical range to which our data are sensitive. The PH_3 distribution derived by Courtin *et al.* (1984) with a constant mixing ratio up to the 3-mbar level appears as a uniform mixing ratio in the pressure regime of this graph; it is given by the dashed-dotted line. The PH_3 distribution derived from the ISO SWS spectrum of Saturn (de Graauw *et al.* 1997) is shown by the dashed line.

Figure 8. Spectra of the models shown in Fig. 7 with our data. The same linetype for each model is used as in Fig. 7.

Figure 9. Vertical distributions of PH_3 . The standard model is displayed as in Fig. 7. The vertical distribution of PH_3 derived by Noll and Larson (1990) is given by the dashed line. A modification that fits our data better is shown by the dashed-dotted line.

Figure 10. Spectra of the models shown in Fig. 9 with our data. The same linetype for each model is used as in Fig. 9. Where not apparent, the dashed-dotted line indicating our modification of the Noll and Larson profile is indistinguishable from our standard model.

Figure 11. Loss profiles corresponding to reactions as shown (reactions R1, R2 and R3 in the text) that are responsible for removing PH_3 from the upper troposphere. The profiles shown correspond to the steady-state solutions for the $K_0 = 1 \times 10^5 \text{ cm}^2 \text{ sec}^{-1}$ case in Fig. 12, but they do not vary significantly among the different cases shown in that figure.

Figure 12. Vertical profile of the PH_3 mixing ratio as a function of the eddy diffusion coefficient in the upper troposphere for the form given in the legend. The symbol ρ denotes density. Our standard model is given by the solid, bold line. The models shown represent the best fit to the spectral data of both the (maximum) mixing ratio at 630 mbar and the eddy diffusion coefficient for each case. The uncertainty of the eddy diffusion coefficient is estimated as a factor of ~ 5 .

Figure 13. Spectra of the models shown in Fig. 12 with our data, using the same linestyle as each model in that figure.

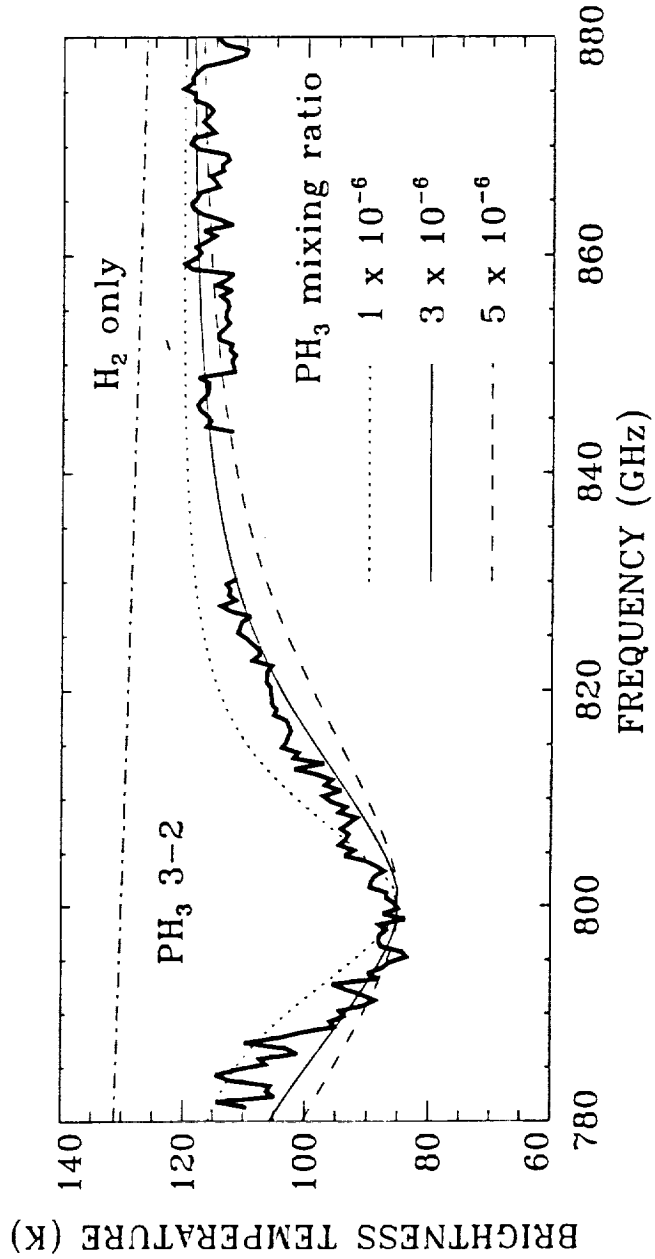
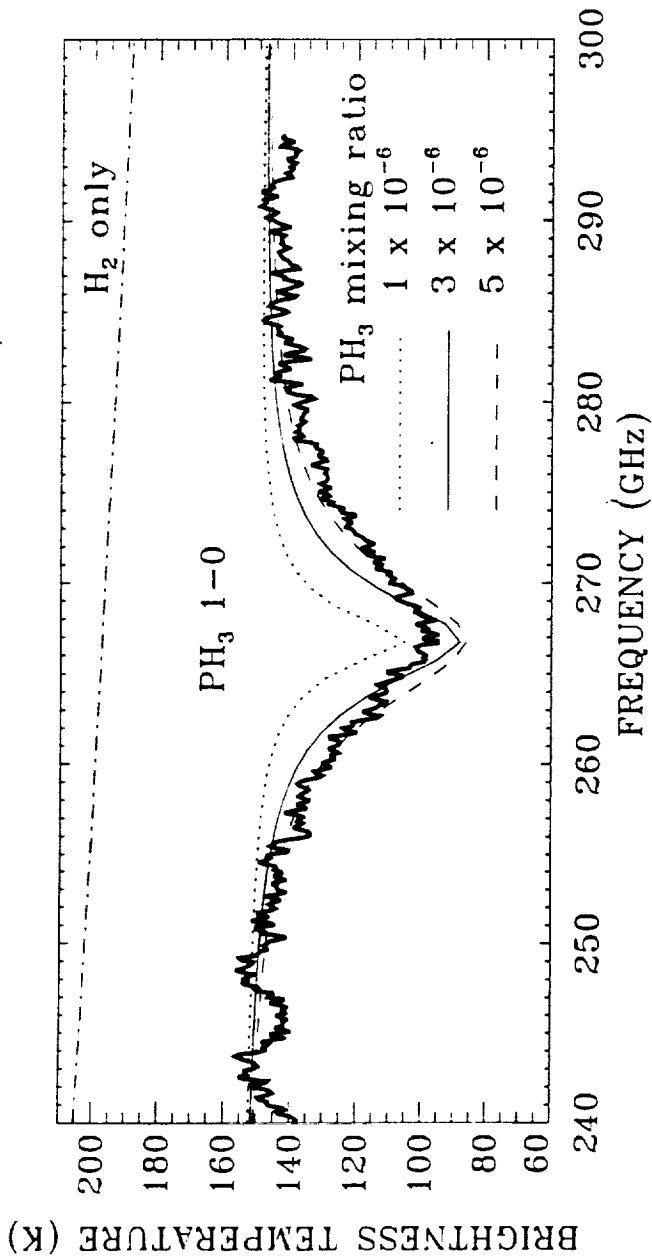


Figure 1

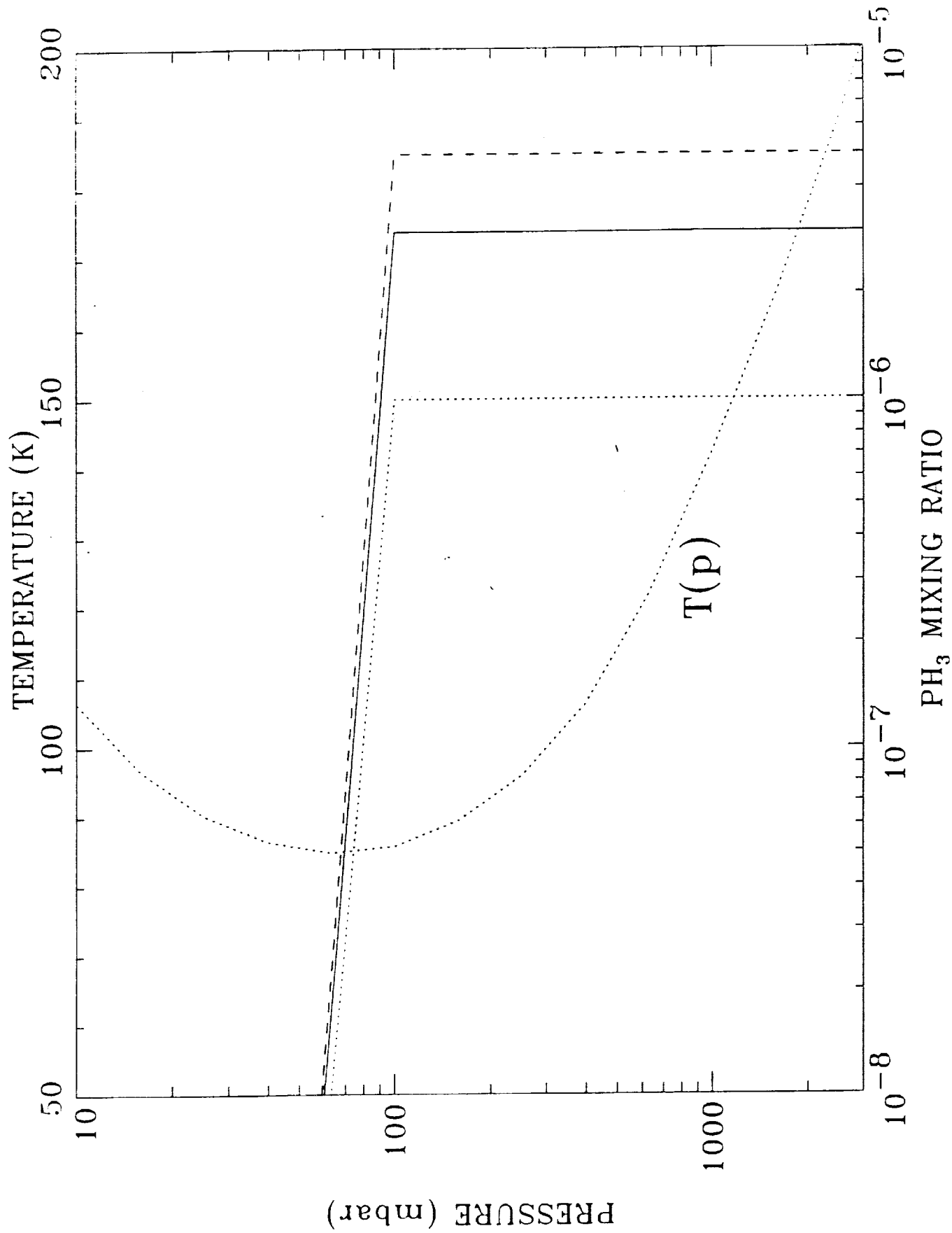


Figure 2

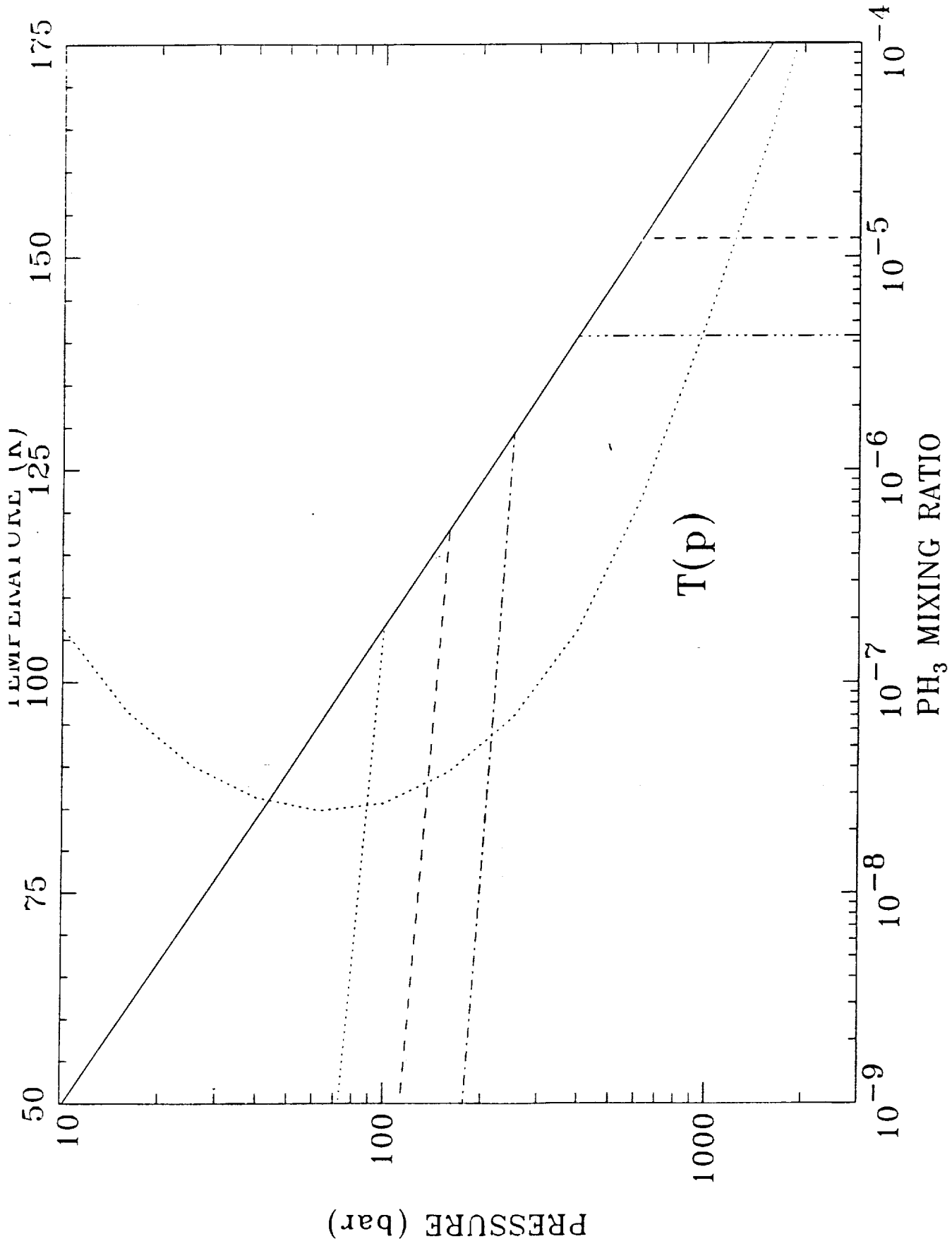


Figure 3

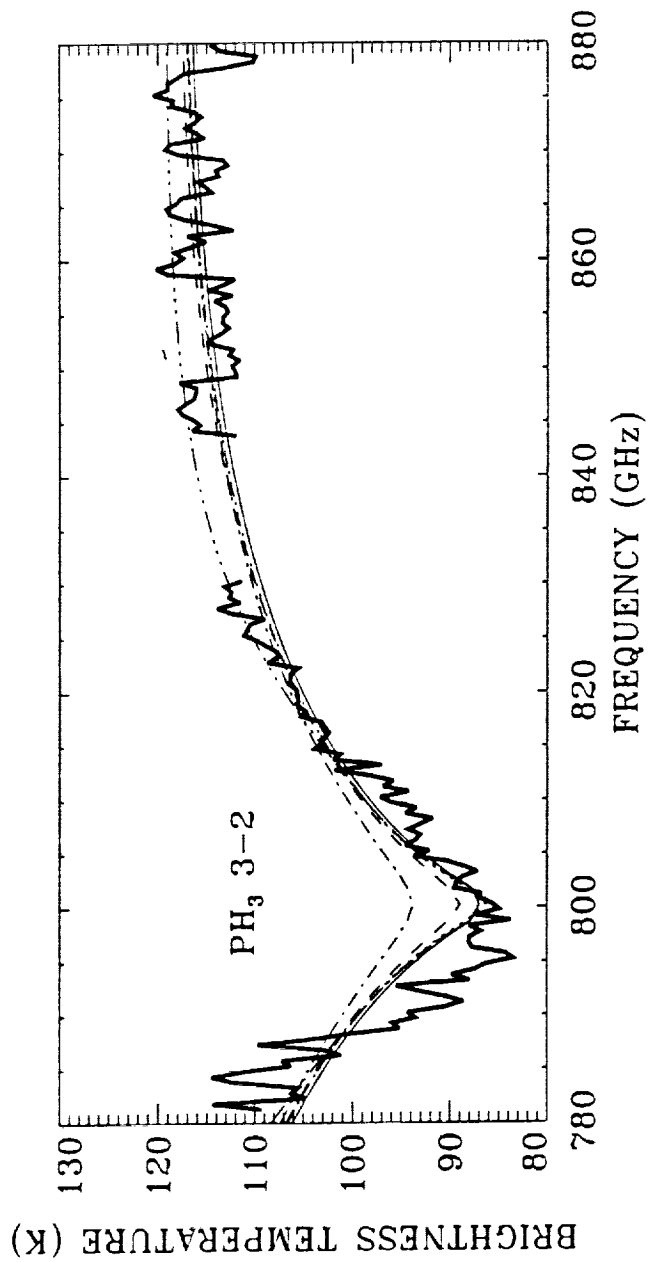
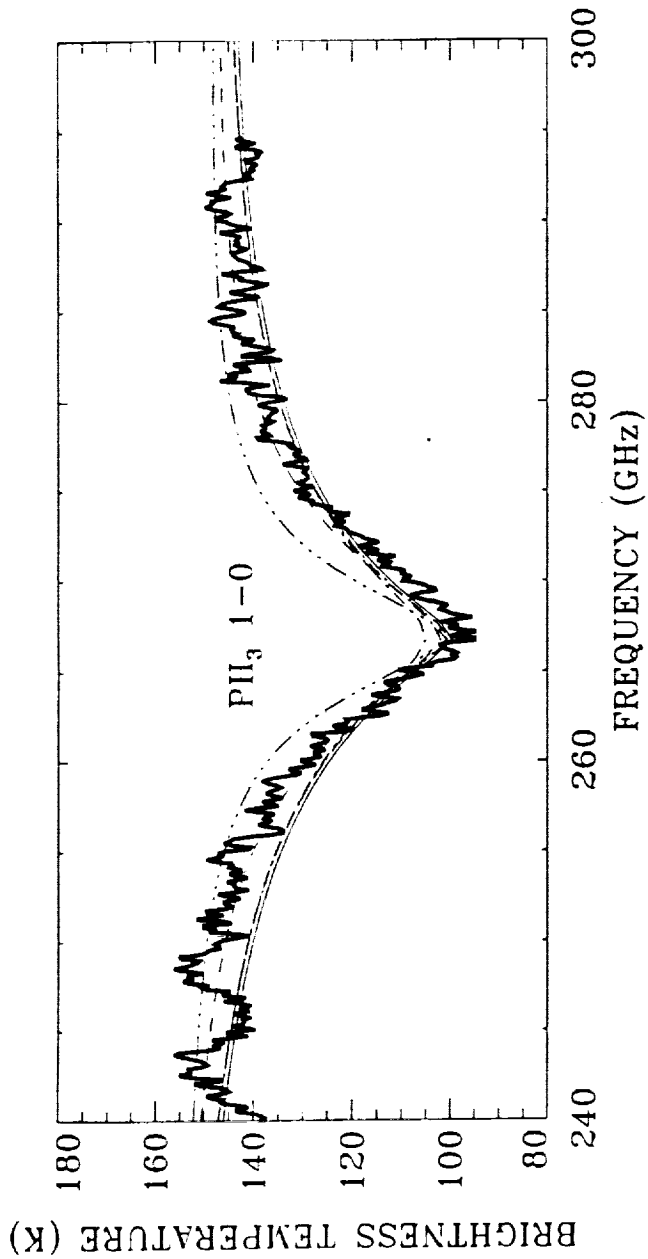
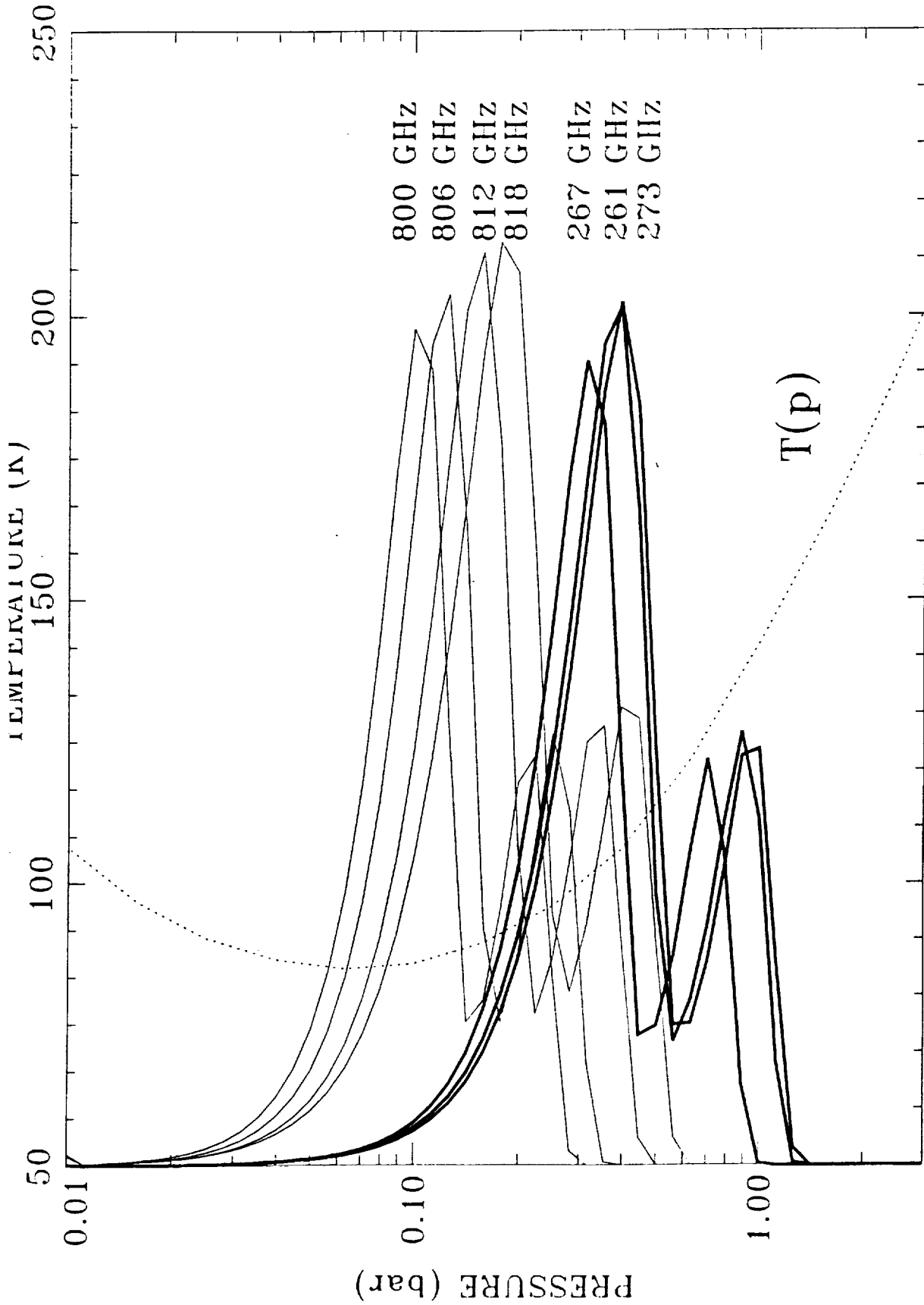


Figure 4



WEIGHTING FUNCTIONS (ARBITRARY UNITS)

Figure 5

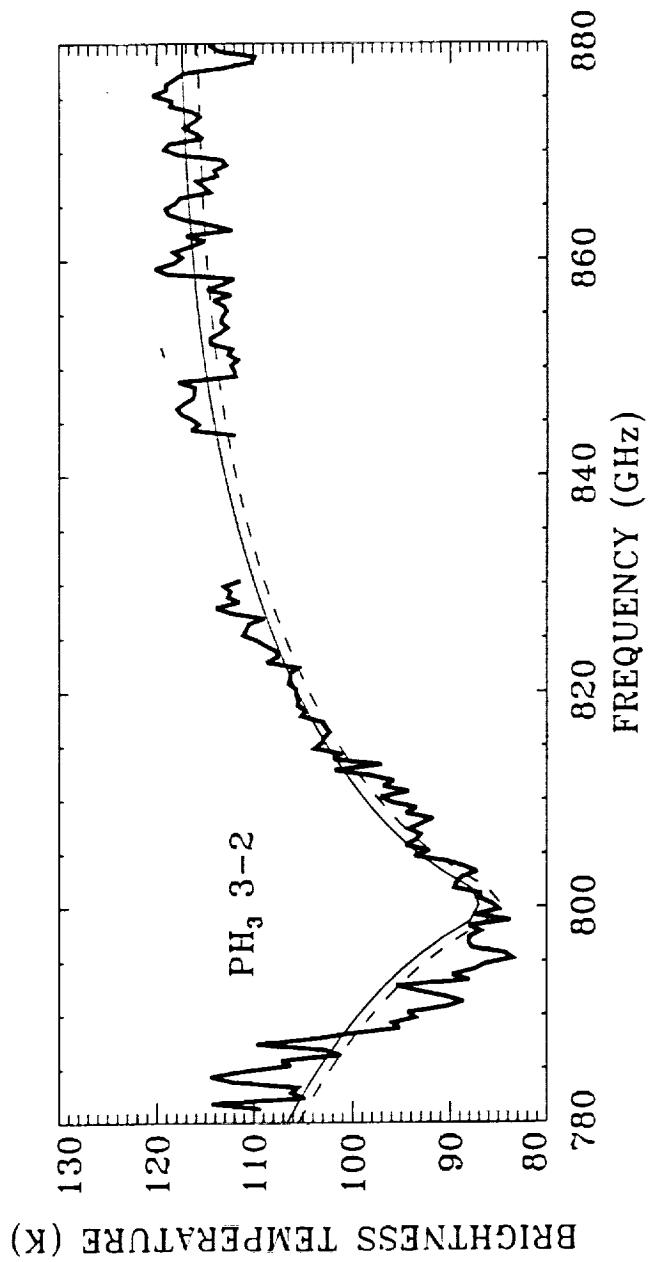
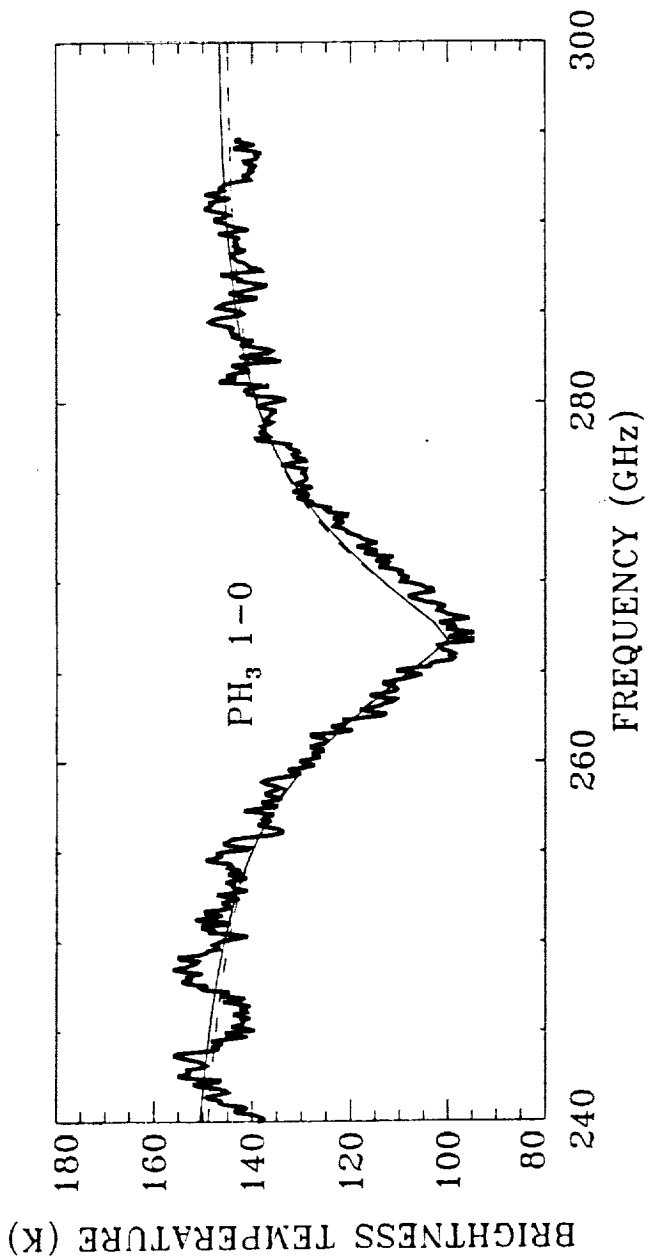


Figure 6

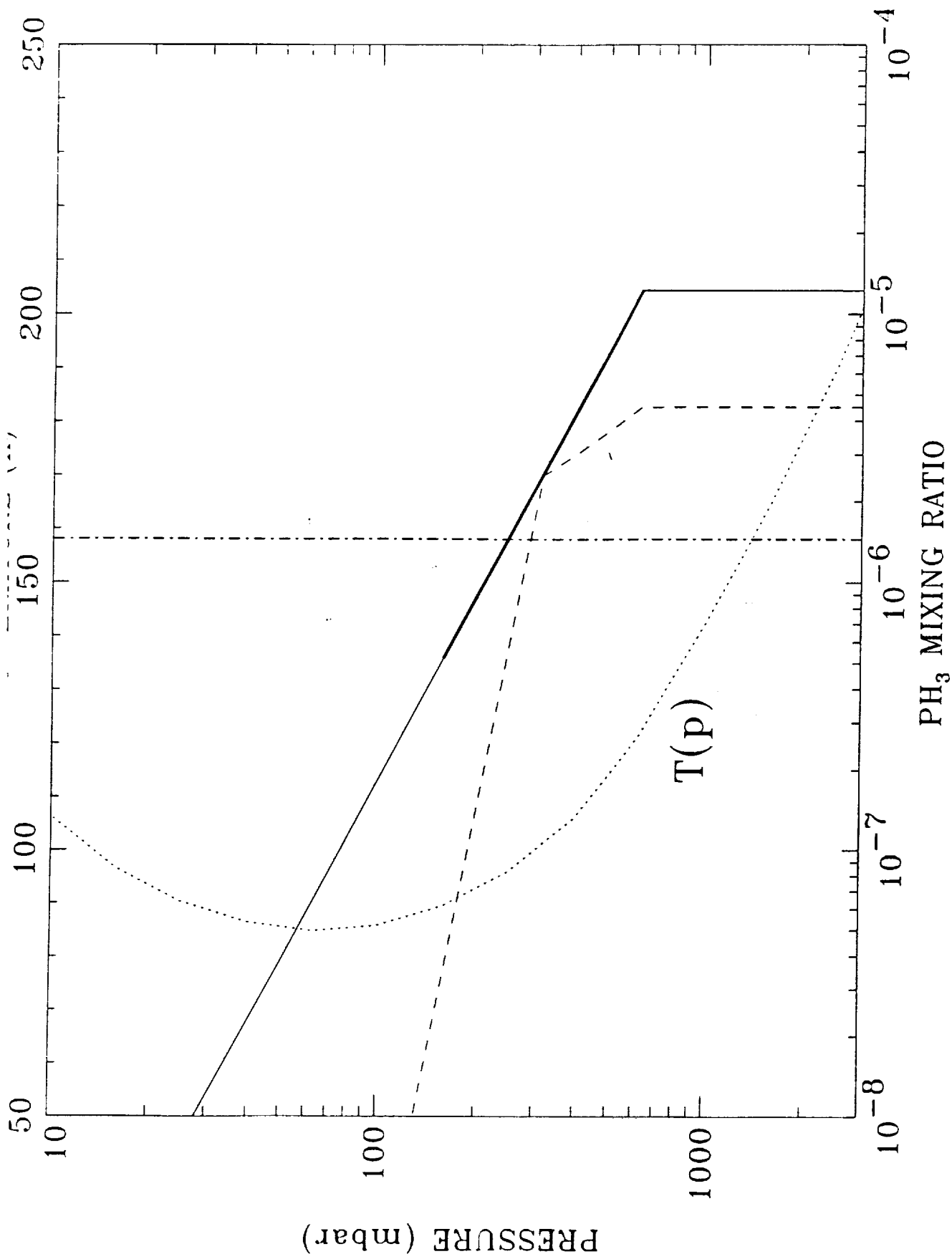


Figure 7

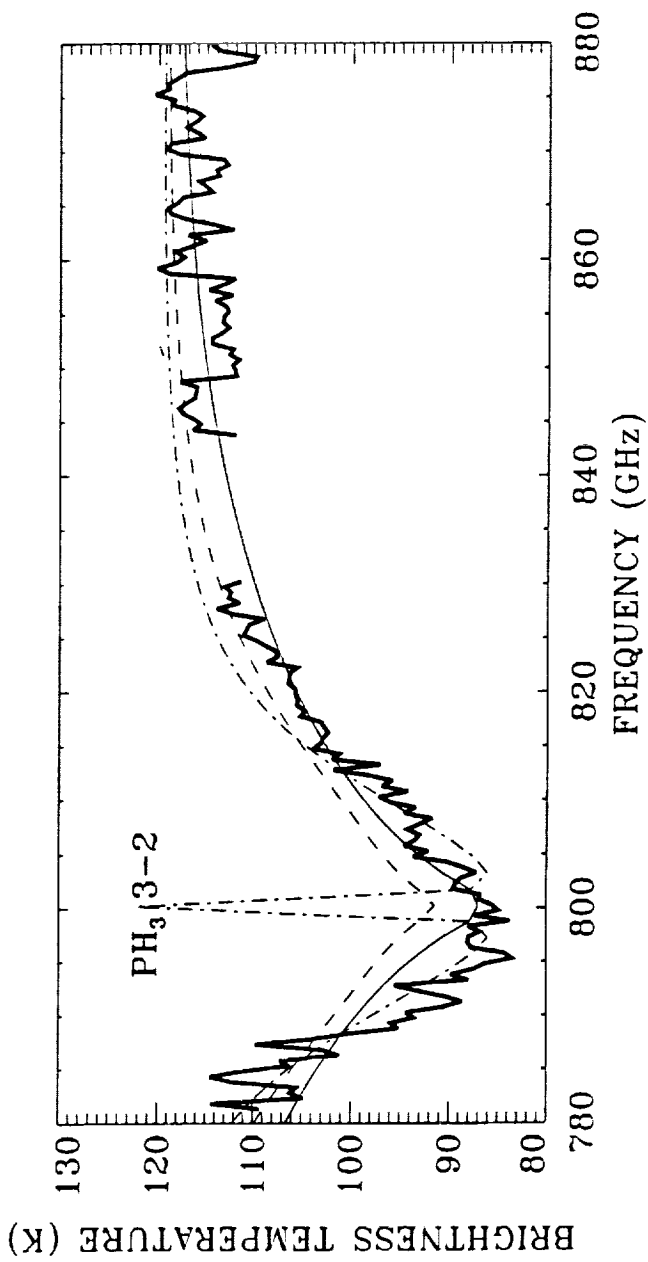
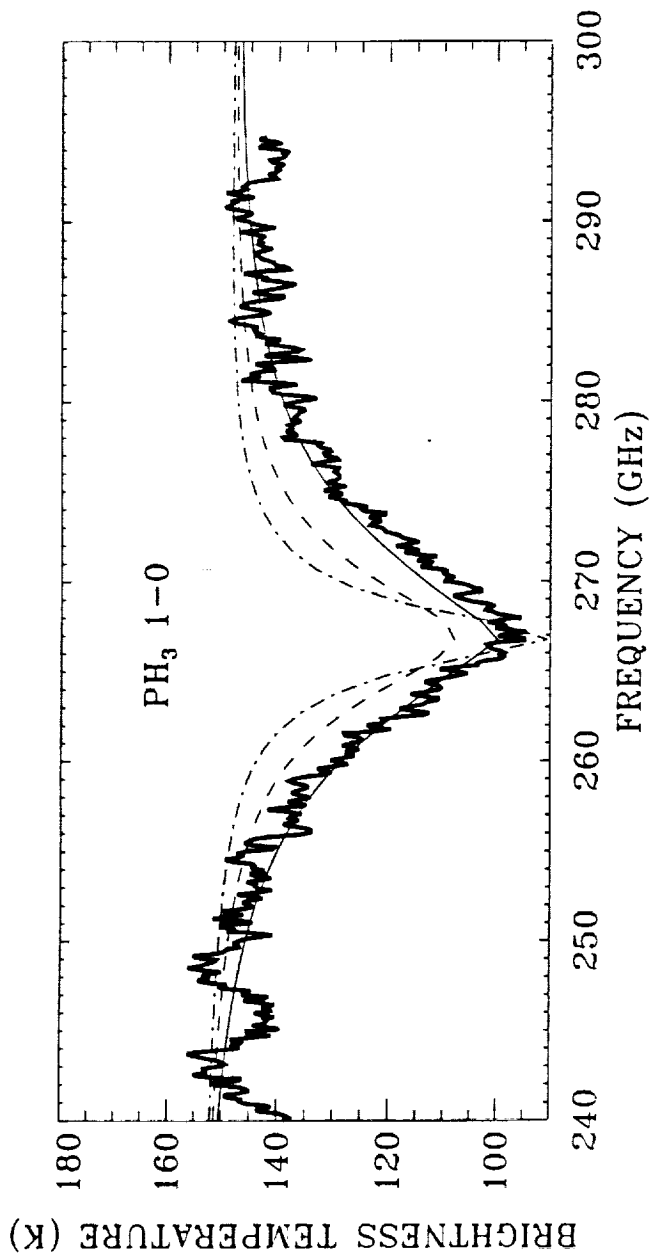


Figure 8

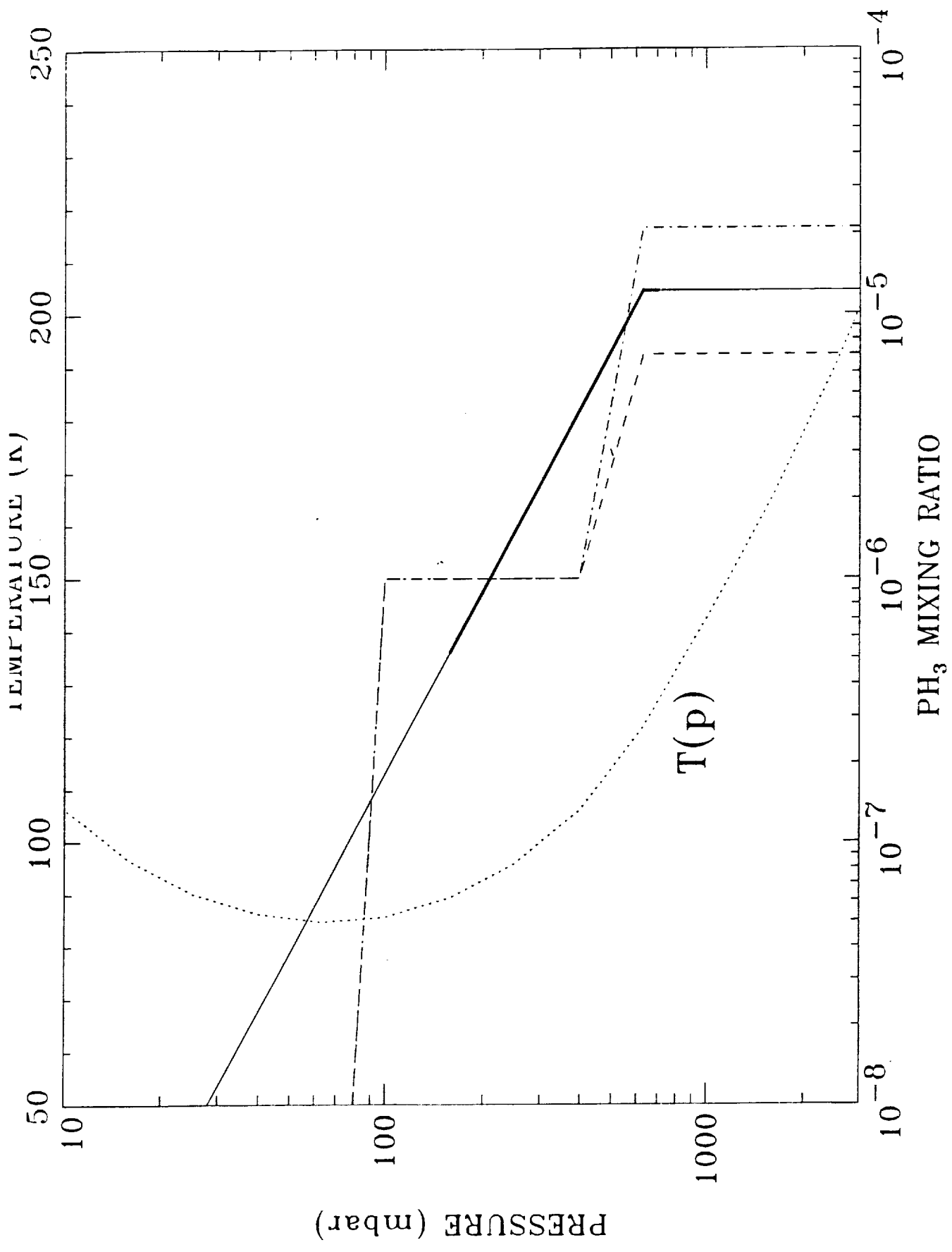


Figure 9

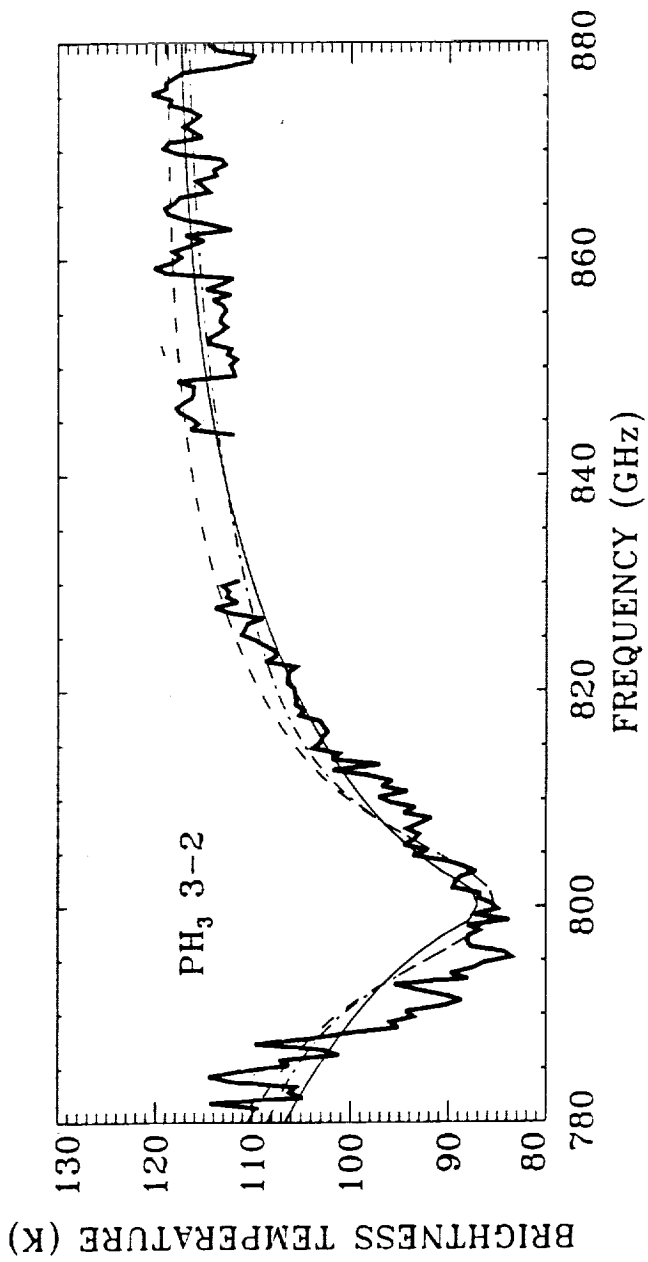
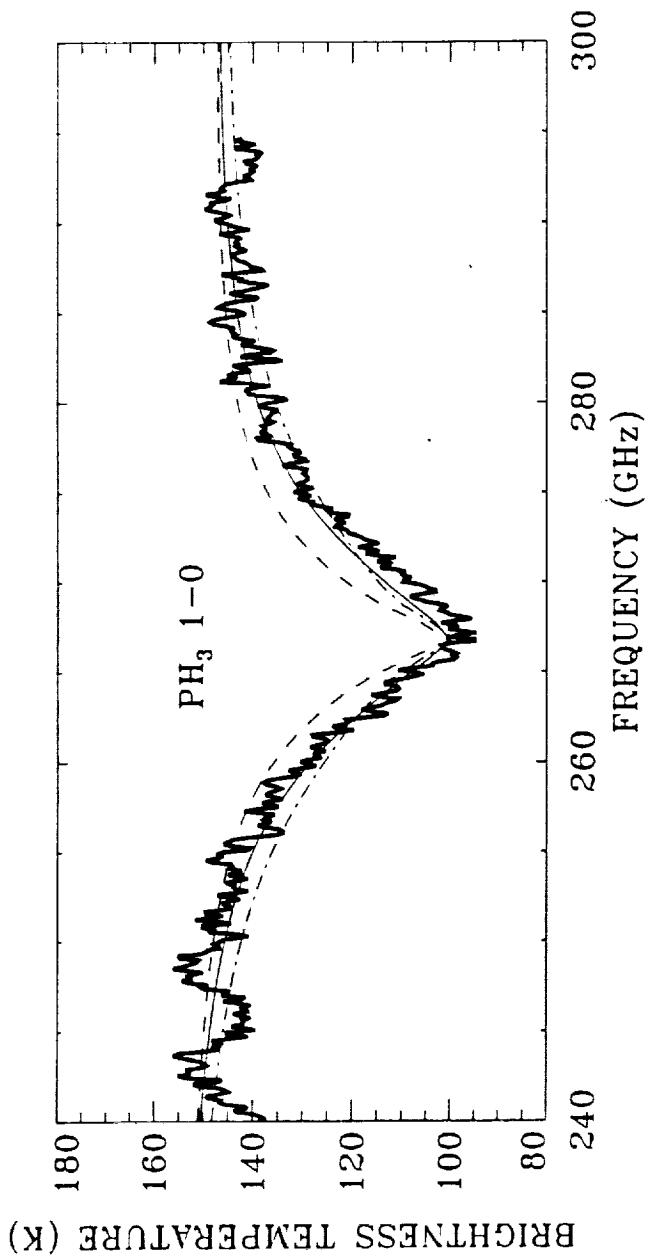


Figure 10

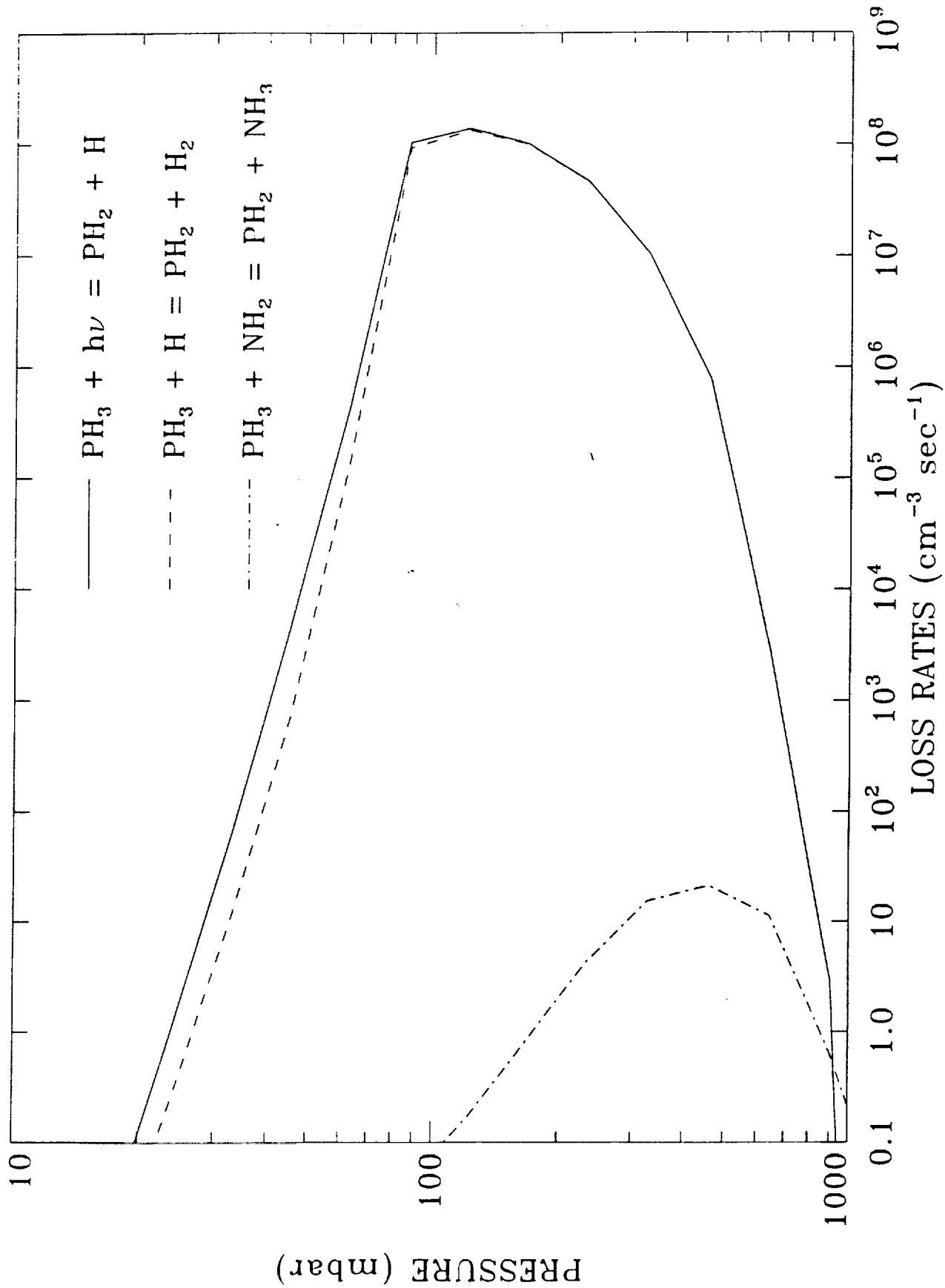


Figure 11

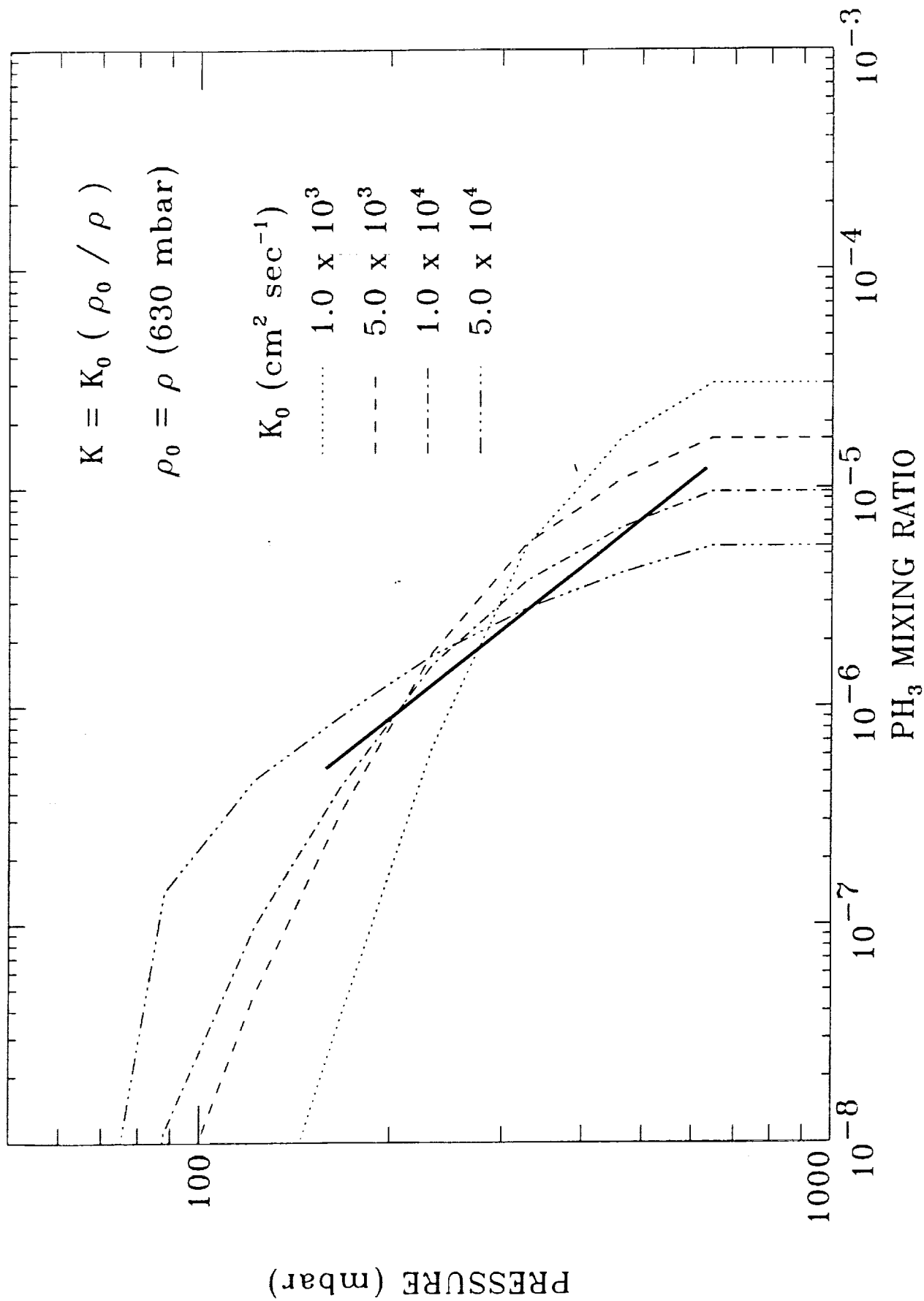


Figure 12

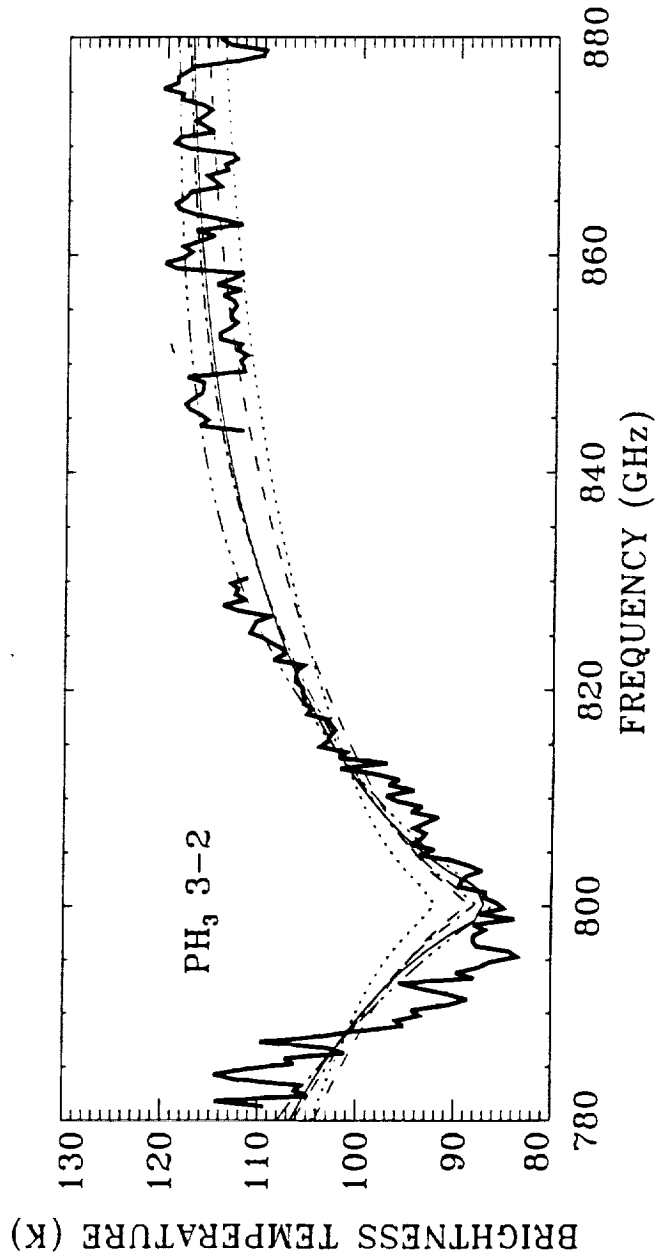
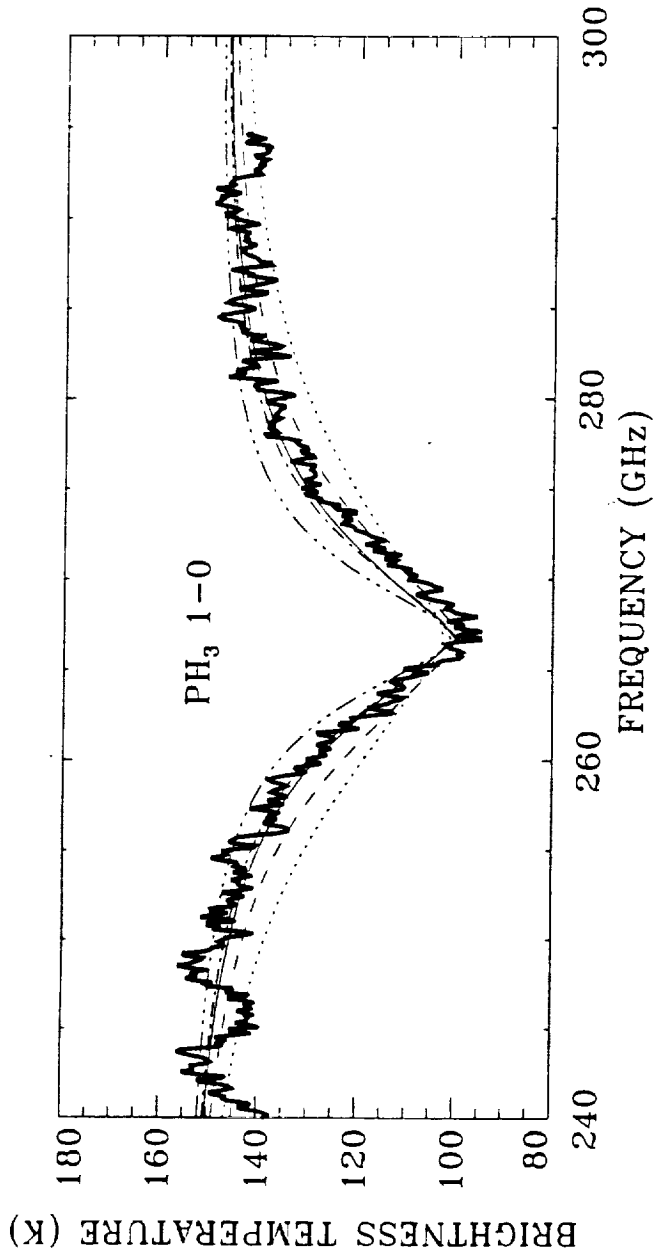


Figure 13

